Progress and Prospects of Inorganic Solid-State Electrolyte-Based All-Solid-State Pouch Cells

Changhong Wang[1,2], Jung Tae Kim[1], Chunsheng Wang[2,*], Xueliang Sun[1,*]

1. Department of Mechanical and Materials Engineering, University of Western Ontario, 1151 Richmond St., London, Ontario, N6A 3K7, Canada

2. Department of Chemical and Biomolecular Engineering, University of Maryland, College Park, MD 20740, USA

*Corresponding author: cswang@umd.edu; xsun9@uwo.ca

Abstract

All-solid-state batteries (ASSBs) have piqued global research interest because of their unprecedented safety and high energy density. Significant advances have been made in achieving high room-temperature ionic conductivity and good air stability of solid-state electrolytes (SSEs), mitigating the challenges at the electrode-electrolyte interface, and developing feasible manufacturing processes. Along with the advances in fundamental study, all-solid-state pouch cells using inorganic SSEs have been widely demonstrated, revealing their immense potential for industrialization. This Review provides an overview of inorganic all-solid-state pouch cells, focusing on ultrathin solid-state electrolyte membranes, sheet-type thick solid-state electrodes, and bipolar stacking. Moreover, several critical parameters directly influencing the energy density of all-solid-state Li-ion and Li-S pouch cells are outlined. Finally, perspectives on all-solid-state pouch cells are provided and specific metrics to meet certain energy density targets are specified. With this Review, we look to facilitate the development of inorganic all-solid-state pouch cells with high energy density and excellent safety.

1. Introduction

Over the past few decades, lithium-ion batteries (LIBs) based on intercalation/de-intercalation chemistry have played an essential role in both the consumer electronics and electric vehicle industry. With technological advancements, the energy density of commercial LIBs has gradually increased to 260 ~300 Wh.kg^{-1}, and more advanced LIBs with higher energy density (e.g., 350 Wh.kg^{-1}~500 Wh.kg^{-1}) are under development. Though the current and predicted energy densities of LIBs complement a broad range of applications, conventional LIBs pose significant safety concerns that originate from using flammable liquid electrolytes and organic polymeric separators.[1] Therefore, finding new superionic conductors and thermally-stable separators that can eradicate the safety concerns of LIBs is highly desired.

To address the safety issues of LIBs, a major focus has been to develop safe electrolytes and separators, such as aqueous electrolytes,[2] non-flammable electrolytes,[3] high-temperature separators,[4] and solid-state electrolytes (SSEs)[5]. In this regard, all-solid-state batteries based on inorganic SSEs have been deemed a promising solution because of several innate characteristics of inorganic SSEs. **First,** inorganic SSEs have excellent thermal stability, and several SSEs possess similar room-temperature ionic conductivities (i.e., $Li_{10}GeP_2S_{12}$ (12 mS.cm^{-1}), $Li_7P_3S_{11}$ (17 mS.cm^{-1}), $Li_{9.54}Si_{1.74}P_{1.44}S_{11.7}Cl_{0.3}$ (25 mS.cm^{-1}) as rival conventional liquid electrolytes.[6] **Second**, inorganic SSEs have a high Young's modulus and transference number, which can potentially prevent lithium dendrite-induced failures.[7] **Third**, the non-fluidity of SSEs can enable ASSBs with bi-polar stacking, which is beneficial for achieving high system-level energy density (particularly volumetric energy density).[8]

Inspired by these advantages, both academic and industrial sectors have devoted many resources to developing ASSBs, from materials synthesis and interface design to practical all-solid-state pouch cell demonstration. **Regarding materials synthesis,** various SSEs including sulfides, oxides, halides, and solid polymers have already exhibited ultrahigh ionic conductivity, wide electrochemical stability windows, and suitable mechanical properties.[9] In addition, their scalability and viability for large-scale mass production have been carefully examined.[10, 11] A recent study shows that processing sulfide SSE in a dry room with a dew point of -40°C can ensure workers' safety and product quality.[12] **As for interface design**, various strategies such as interface modification and solid electrolyte interphases (SEI) design have been proven effective in suppressing interfacial side reactions, suppressing

dendrite growth,[13] and improving interfacial solid-solid ionic contact.[14] Furthermore, several key technical factors such as pressure, temperature, testing protocol, and bipolar stacking have been optimized to obtain the high performance of ASSBs.[15] Using these technological advances, lab-level ASSBs have already demonstrated impressive electrochemical performance, such as ultra-long cycling stability (> 3000 cycles with 80% capacity retention),[16] high power density (1000C), and high output voltage realized by bipolar stacking (> 12V). In parallel, all-solid-state pouch cells have also been demonstrated, exhibiting satisfactory electrochemical performance and high feasibility for commercialization. These lab-scale demonstrations have given rise to various start-up companies (e.g., Quantum Scape, Solid Power) and even prompted several legacy companies (e.g., Toyota, Samsung) to develop ASSBs. The abundance of review papers that discuss the fundamental challenges and strategies of ASSBs,[17-19, 20] especially in recent years, clearly manifests the paradigm shift in the energy storage field towards ASSB configurations. However, few of them focus on practical all-solid-state pouch cells, particularly with inorganic SSEs, which are far more difficult to integrate into pouch cells than organic solid polymer electrolytes,

In this Review, we summarize the recent progress of all-solid-state pouch cells using inorganic SSEs and highlight the various challenges of fabricating their essential components, such as ultrathin SSE membranes and sheet-type solid-state electrodes. Furthermore, state-of-the-art fabrication methods are discussed and comparatively analyzed. To facilitate the commercialization of ASSBs and link fundamental research with practical application, we numerically examine critical parameters that directly influence the energy density of all-solid-state pouch cells, including SSE thickness, the areal capacity of solid-state electrodes, N/P ratio, and Li metal thickness. Moreover, a set of metrics are provided to meet the energy density targets. Finally, promising directions and feasible strategies to realize all-solid-state pouch cells are highlighted. This Review seeks to guide the research and development of inorganic SSE-based all-solid-state pouch cells with high energy density and inherent safety.

2.1 Roadmap of all-solid-state pouch cells with inorganic solid-state electrolytes
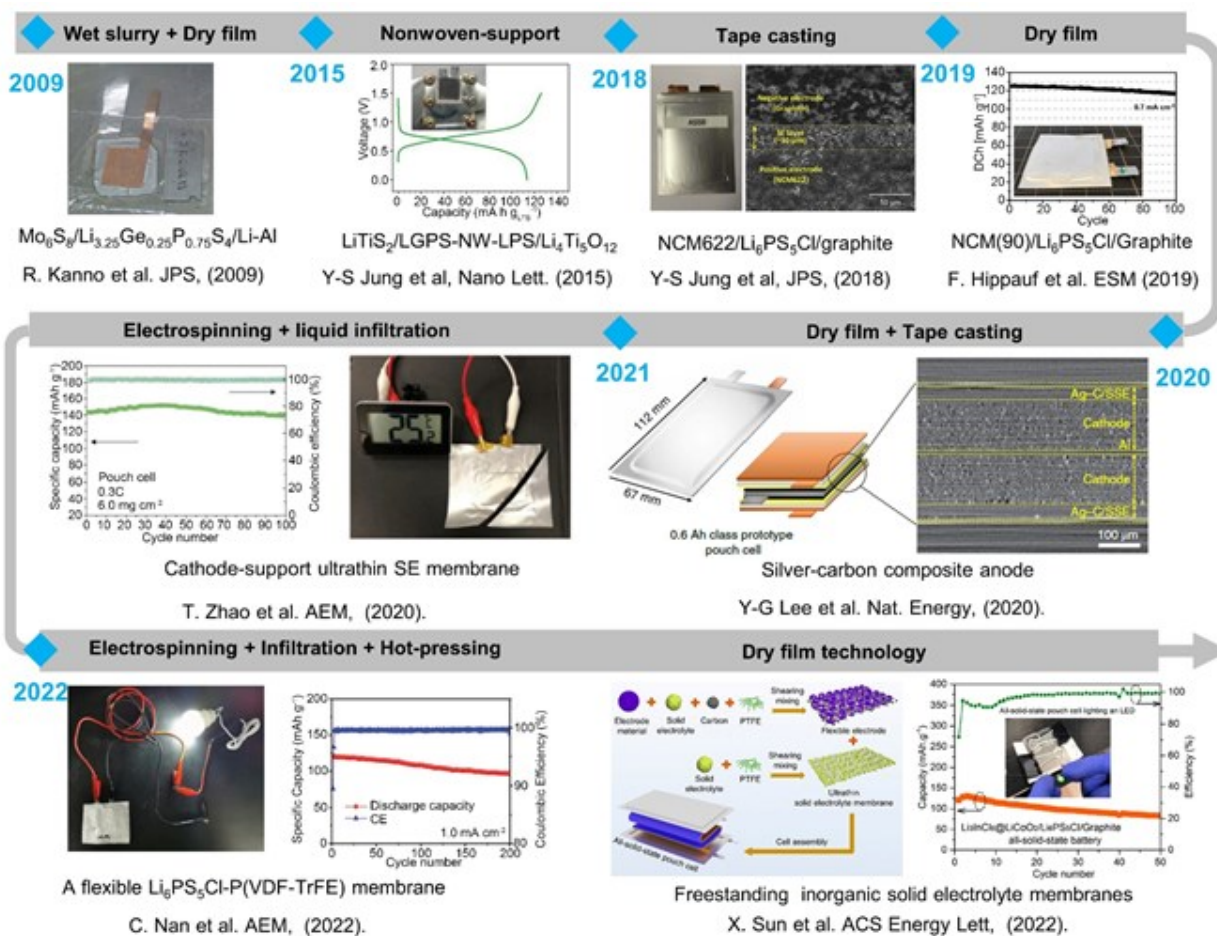
Figure 1. **Roadmap of inorganic all-solid-state pouch cells**. Figures are adapted from references with permissions from refs.[21-28]

In 2009, R. Kanno et al. developed the first 30×30 mm^2 all-solid-state pouch cell prototype (**Figure 1**), demonstrating high cycling stability at a current of 0.1 mA.[21] In 2015, Y-S Jung et al. developed a bendable and thin SSE membrane reinforced with a mechanically compliant poly(paraphenylene terephthalamide) nonwoven (NW) substrate. Coupled with LiTiS$_2$ and Li$_4$Ti$_5$O$_{12}$ electrodes, a sheet-type all-solid-state pouch cell was demonstrated.[22] In 2017, a practical slurry coating process was reported, which uses styrene-butadiene-based binders (i.e., styrene ethylene butylene styrene copolymer (SEBS) and styrene butadiene styrene copolymer(SBS)) and non-polar solvents (i.e., heptane for SEBS and anisole for SBS). Based on this process, sheet-type all-solid-state pouch cells with a reversible areal capacity of 1.5 mAh.cm^{-2} was demonstrated.[29] To facilitate the fabrication of sheet-type solid-state electrodes, Y-S Jung's group developed various soluble SSEs, such as Li$_4$SnS$_4$-

LiI,[30] Li_6PS_5Cl,[31, 32] $Li_6PS_5Cl_{0.5}Br_{0.5}$.[33] These soluble SSEs can easily infiltrate conventional sheet-type electrodes, enabling easier solid-state battery manufacturing.[31] In 2018, a tape-casting process was developed to fabricate all-solid-state pouch cells.[34, 35] A 80×60 mm^2 NCM622/graphite solid-state pouch cell fabricated by the slurry coating process showed a high cell-based energy density of 184 Wh.kg^{-1} and a volumetric energy density of 432 Wh. L^{-1}.[35] Following this work, more studies that use the slurry coating process to fabricate all-solid-state pouch cells have been reported, paving the way for the large-scale production of ASSBs.[23, 36, 37] However, some inorganic SSEs, such as sulfides and halides, are chemically sensitive to polar solvents and binders. Therefore, a solvent-free dry film process to fabricate solid-state sheet-type electrodes and ultrathin SSE membranes is highly desired. In 2019, F. Hippauf et al. developed a solvent-free dry film process using polytetrafluoroethylene (PTFE),[24] enabling a 3×3 cm^2 all-solid-state pouch cell that can stably cycle for 100 cycles. Following this work, Samsung Advanced Institute of Technology (SAIT) developed a 0.6 Ah pouch cell using silver-carbon composites as the anode and a high-Ni cathode (Li_2O-ZrO_2-coated $LiNi_{0.9}Mn_{0.05}Co_{0.05}O_2$), fabricated using both the tape casting process and the dry film method. This work represents a significant milestone for inorganic all-solid-state pouch cells.[25] Our group also developed a solvent-free method to fabricate halide-based all-solid-state pouch cells with a configuration $Li_3InCl_6@LiCoO_2/Li_3InCl_6+Li_6PS_5Cl/graphite@Li_6PS_5Cl$, delivering an initial capacity of 121.2 mAh g^{-1} and a capacity of 83.1 mAh.g^{-1} after 50 cycles.[28] Moreover, T. Zhao's group demonstrated a scalable cathode-supported fabrication process where an ultrathin and robust SSE film was directly coated on top of the cathode layer in 2021. This integrated cathode/SSE process enables an intimate interface and continuous Li-ion transport within entire electrodes.[26] Recently (in 2022), C. Nan et al. fabricated a thin (30~40μm) and flexible Li_6PS_5Cl membrane via an electrospinning-infiltration-hot-pressing method. Coupled with an NMC811 cathode, a 6×6 cm^2 all-solid-state pouch cell delivered a high-capacity retention of 81% after 200 cycles at 1.0 mA.cm^{-2}. As endeavors to develop all-solid-state pouch cells continue, a viable path toward their commercialization will become clearer.

2.2 Fabrication of ultrathin yet robust inorganic solid-state electrolyte membranes

Arguably, the SSE membrane is the most crucial component in an all-solid-state pouch cell. Developing feasible methods that can be used to fabricate ultrathin yet robust SSE membranes is critical to enable large-scale processing and manufacturing of all-solid-state pouch cells.[38] In contrast to solid polymer electrolytes that have innate flexibility, achieving flexible and freestanding inorganic all-solid-state pouch cells is more challenging because of

the fragile nature of inorganic SSEs and their chemical vulnerability with polar solvents and polymeric binders.

To overcome these challenges, substantial efforts have been devoted to screening solvents and binders that are compatible with inorganic SSEs, especially sulfide SSEs. So far, various methods including tape casting,[39, 40] solution infiltration,[33] dry film technology,[24, 28, 41] vacuum infiltration,[42] hot/cold press with polymers,[43, 44] and 3D printing.[45] have been applied to fabricate ultrathin SSE membranes. The recent progress of ultrathin SSE membranes has been reviewed.[19] **Table 1** summarizes technologies to fabricate ultrathin SSE membranes. To avoid repetition, we highlight several typical SSE membrane fabrication methods compatible with large-scale roll-to-roll manufacturing processes (**Figure 2**).

Table 1. The thickness of ultrathin SSE membranes fabricated by different methods

| Solid-State Electrolyte	Binder/Solvent	SSE membrane thickness (μm)	Ionic conductivity at room temperature (S.cm^{-1})	Fabrication Method	Ref.
$Li_{6.5}La_3Zr_{1.5}Ta_{0.5}O_{12}$	Polyvinylpyrrolidone (PVP)/isopropanol	10~100	1.0×10^{-3}	Printing and rapid sintering	[45]
Li_6PS_5Cl	Polydopamine	35	2.0×10^{-4}	Cold pressing	[43]
Li_6PS_5Cl	Polyethylene oxide	65	2.83×10^{-4} (40°C)	Wet-slurry coating	[46]
β-Li_3PS_4	Acetonitrile	8 ~50	1.2×10^{-4}	evaporation-induced self-assembly (dip-coating)	[47]
β-Li_3PS_4	Acetonitrile	6~35	7.2×10^{-4}	dip coating+hot press	[48]
$Li_7P_3S_{11}$	SEBS/xylene	~50	7.0×10^{-4}	Tape casting	[49]
$Li_{6.5}La_3Zr_{1.5}Ta_{0.5}O_{12}$	Polytetrafluoroethylene (PTFE)	100	1.2×10^{-4}	Solvent-free process	[41]
$77.5Li_2S–22.5P_2S_5$	Seal-healing polymers	64	1.0×10^{-4}	Hot press	[44]
Li_3InCl_6	Polytetrafluoroethylene (PTFE)	15	1.0×10^{-3}	Solvent-free process	[28]

$Li_{0.34}La_{0.56}TiO_3$	polyvinyl butyral (PVP) and butyl benzyl phthalate (BBP)	25	2.0×10^{-5}	Tape casting	[39]
$Li_6PS_5Cl_{0.5}Br_{0.5}$	anhydrous EtOH	40–70	2.0×10^{-3}	Solution infiltration	[33]
$Li_{5.4}PS_{4.4}Cl_{1.6}$	Polytetrafluoroethylene (PTFE)	30	8.4×10^{-3}	Solvent-free process	[50]
$Li_3OCl_{0.5}Br_{0.5}$	NBR-dibromoethane	310	2.6×10^{-5}	Tape casting	[51]
LLTO/PVDF	Polyvinylidene fluoride (PVDF)/NMP	9.6	4.7×10^{-4}	Tape casting	[40]
Li_6PS_5Cl	Silicon-rubber-chloroform cellulose	70	6.3×10^{-3}	Tape casting+infiltration	[52]

Tape casting is a feasible method widely used to fabricate thin SSE membranes. For example, H. Wang et al. prepared large-sheet perovskite-type $Li_{0.34}La_{0.56}TiO_3$ membranes on a polyethylene terephthalate (PET) substrate via a tape-casting process (**Fig. 2A**).[39] In this approach, the PET substrate should be removed when integrating the SSE membrane into practical large-format pouch cells, which is not beneficial for forming intimate electrode-electrolyte interface contact. To avoid such a drawback, a cathode-supported SSE membrane was fabricated to reinforce interfacial adhesion and minimize interfacial ion transport resistance between the electrode and SSE (**Fig. 2B**).[26, 53] M. Doeff et al. developed a scalable freeze-tape casting process to fabricate three-dimensional porous LLZO, which can be potentially used for cathode composites in ASSBs.[54] In addition, M. Finsterbusch et al. presented a water-based tape-casting process for garnet-supported solid-state lithium batteries featuring a LiFePO$_4$-poly(ethylene oxide) (PEO) composite cathode, which delivered a high capacity of 136 mAh.g^{-1} with good cycling stability for 50 cycles. Water-based tape casting represents an economically and environmentally benign path, which is highly desired for the large-scale production of ASSBs. Therefore, more efforts are encouraged to develop greener, safer, and cheaper manufacture for ASSBs.[55]

SSE solution infiltration into a flexible substrate is another strategy to obtain ultrathin SSE membranes. Many sulfide SSEs can be dispersed into some organic solvents (i.e., tetrahydrofuran (THF), acetonitrile (ACN), ethyl acetate (EA)) to form an SSE suspension or

dissolved in some strong polar solvents (i.e., methanol, ethanol, N-methyl formamide (NMF)) to form a homogenous SSE solution.[30, 48, 56] This liquid-processable strategy opens an avenue for producing SSE membranes via infiltrating SSE into flexible porous substrates and removing organic solvents by heating. Some examples include Li_4SnS_4-LiI,[30] Li_6PS_5Cl,[31, 32] and $Li_6PS_5Cl_{0.5}Br_{0.5}$.[33] A typical example is infiltrating soluble-processable $Li_6PS_5Cl_{0.5}Br_{0.5}$ into an electrospun polyimide (PI) substrate (**Fig. 2C**). Due to the high thermal stability of PI and inorganic SSE, as-prepared 40μm membranes are thermally stable up to 500°C and exhibit a high ionic conductivity of 2.0 mS.cm^{-1} (**Fig. 2D**).[33] In addition, a thin (30~40 μm) Li_6PS_5Cl membrane was fabricated via an electrospinning-infiltration-hot-pressing method (**Fig. 2E**).[27] The interaction between Li_6PS_5Cl and polymeric framework (poly(vinylidene fluoride-co-trifluoro ethylene, P(VDF-TrFE)) ensures a high room-temperature ionic conductivity of 1.2 mS.cm^{-1} and excellent mechanical ductility. The resulting ASSBs demonstrated high capacity retention of 92% after 1000 cycles and 71% after 20000 cycles at 1.0 mA.cm^{-2} at room temperature.
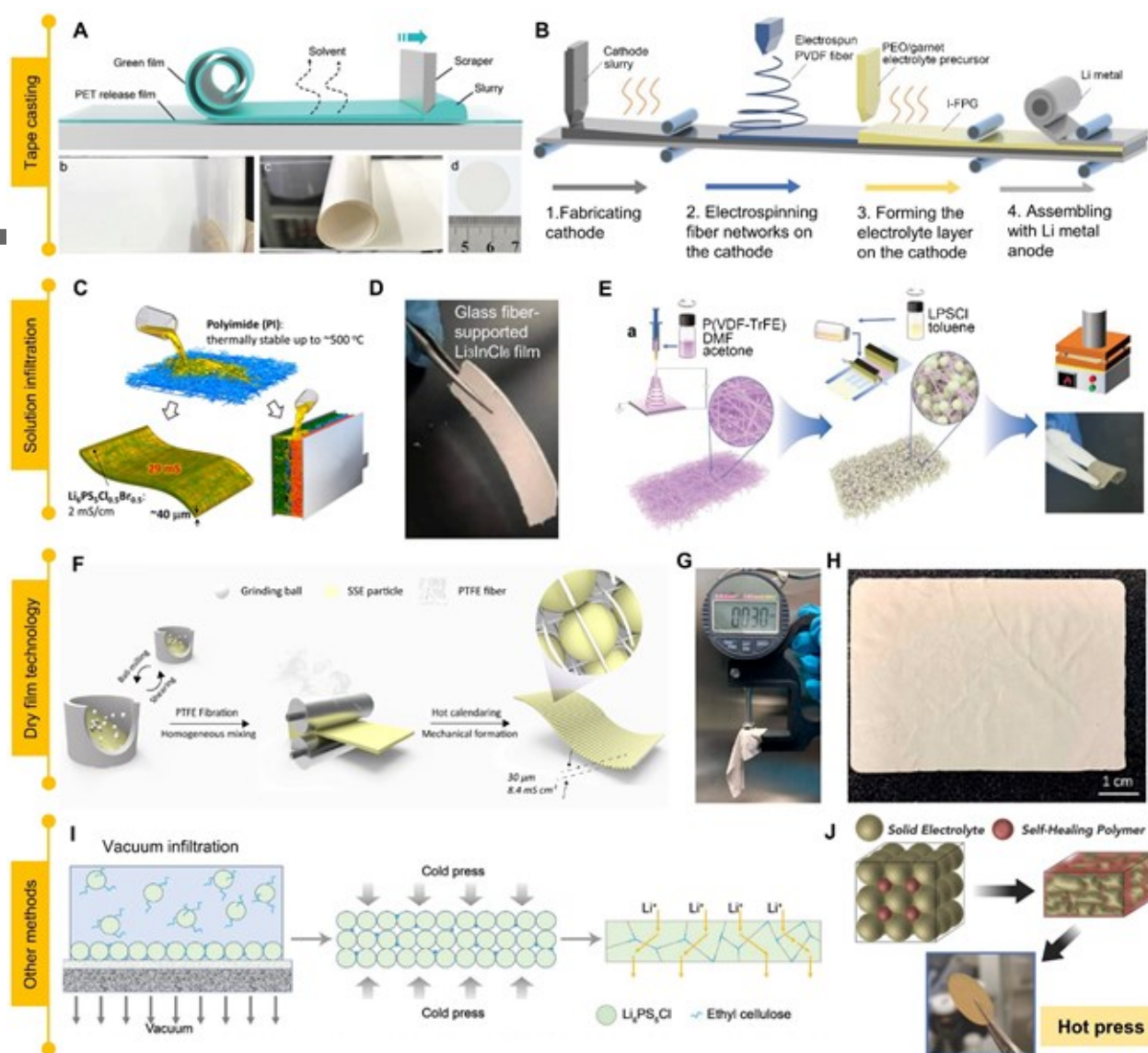
Figure 2. Various strategies to fabricate thin inorganic solid-state electrolyte membranes. (**A**) Schematic for preparation of LLTO film using a tape-casting method, adapted with permission from ref.[39], Copyright©2020, Wiley. (**B**) Schematic of the continuous manufacturing process of cathode-supported ultrathin SSE membranes for ASSBs. Adapted with permission from ref.[26] . Copyright©2021, Wiley. (**C**) the infiltration of sulfide electrolyte solution into a polyimide substrate. Adapted with permission from ref.[33] Copyright©2021, American Chemical Society. (**D**) A thin Li_3InCl_6 membrane was fabricated by infiltrating its solution into a glass fiber substrate. Adapted with permission from ref.[57]. Copyright@2022, Elesvier. (**E**) Schematic illustration for the fabrication

procedure of the interpenetrating LPSCl@P(VDF-TrFE) CSEs via an electrospinning-infiltration-hot-pressing method. Adapted with permission from ref.[27] Copyright©2022, Wiley. (**F**) A schematic illustration of the dry-film process for fabricating SSE membranes. (**G**) A digital photo showing SSE thickness and final status (**H**). Adapted with permission from ref.[50] Copyright©2021, ACS. (**I**) Schematic of the binder-assisted vacuum infiltration method in fabricating the thin SE membrane. Adapted with permission from ref.[42] Copyright©2021, Wiley. (**J**) Schematic for forming the SSE membrane with self-healing polymers. Adapted with permission from ref.[44] Copyright©2015. Wiley.

Both the tape casting and SSE infiltration methods are wet-chemistry processes that require excellent (electro)chemical compatibility between SSEs and organic solvents/binders to maintain the high conductivity of the inorganic SSE membranes. However, sulfides and halides SSEs are chemically vulnerable to polar solvents/binders. Therefore, using the wet-chemistry process to develop SSE membranes sometimes decreases the high conductivity of these inorganic SSEs. In the future, it is essential to develop chemically-compatible binders and solvents for processing SSEs without compromising their room-temperature ionic conductivity. In addition, it is worthwhile to investigate why the ionic conductivity of inorganic SSEs obtained by the wet-chemistry method is lower than that via solid-state reactions. This mechanistic insight would accelerate the development of the wet-chemistry process.

Recently, **solvent-free dry film technology** has received increasing attention for fabricating SSE membranes and sheet-type solid-state electrodes because of its advantages concerning environmental friendliness, low cost, enhanced (electro)chemical compatibility, high production efficiency, and enhanced electrode performance.[24, 28, 41, 58, 59] Yao and co-workers reported a 30μm $Li_{5.4}PS_{4.4}Cl_{1.6}$ membrane fabricated by solvent-free dry film approach (**Fig. 2F** and **2G**). The solvent-free fabrication process enables a large dimension of $Li_{5.4}PS_{4.4}Cl_{1.6}$ membrane that exhibits a high room-temperature conductivity of 8.4 mS.cm^{-2} (**Fig. 2H**).[50] In view of the superiorities of solvent-free dry film technology, we also demonstrated several freestanding inorganic SSE membranes ($Li_{6.75}La_3Zr_{1.75}Ta_{0.25}O_{12}$(LLZTO), Li_6PS_5Cl, and Li_3InCl_6) with controllable thicknesses from 15 to 30 μm.[28, 41] To improve the air stability of sulfide SSE membranes, a Li$^+$-conductive superhydrophobic protection layer is spay-coated on a 100 μm Li_6PS_5Cl membrane fabricated by the solvent-free dry film method.[60]

Besides the wet-chemistry approach and dry film technology, a few other methods were also used to fabricate thin SSE membranes. For instance, H. Zhu and co-workers prepared a 47μm freestanding Li_6PS_5Cl membrane using an amphipathic binder (ethyl cellulose) through **vacuum filtration and cold pressing (Fig. 2I)**.[42] Furthermore, a seal-healing polymer was synthesized to fill the pores of cold-pressed SSE pellet (**Fig. 2J**), which not only realizes fast Li-ion transport between inorganic SSE particles but also exhibits excellent mechanical strength. Though several reports demonstrate ultrathin SSE membranes with decent ionic conductivity at room temperature, the mechanical strength of the SSE membrane cannot be overlooked, particularly considering the high-efficiency roll-to-roll manufacturing.[10] To our understanding, the mechanical property of inorganic SSE membranes should be on par with that of commercial Celgard 2400 separators (stress 70 MPa with less than 3% elongation) [61] so that ASSBs can be efficiently produced via the high-throughout roll-to-roll technology.[23] For this purpose, introducing a proper amount of organic polymeric binders seem essential to enable SSE membranes with favorable mechanical properties. However, most polymeric binders used for fabricating inorganic SSE membranes are ionically non-conductive, restricting ion transport between SSE particles and thus decreasing the otherwise high conductivity of the SSE. Therefore, developing ion-conductive binders that are also compatible with SSEs or volatile binders that enable binder-free electrodes is highly desired.[62] [63]. Overall, thin inorganic SSE membranes should simultaneously possess high ionic conductivity, wide electrochemical stability window, excellent mechanical flexibility and strength, low electronic conductivity, and outstanding capability to suppress lithium dendrite formation.

2.3 Fabrication of thick solid-state electrode films

2.3.1 Fabrication methods for thick solid-state electrode film

As crucial as inorganic SSE membranes, solid-state electrodes with a high areal capacity (> 4 mAh.cm^{-2}) are indispensable for all-solid-state pouch cells with high energy density. However, they have been impeded by mainly poor electrode-electrolyte interface contact, significant interfacial side reactions, and poor charge transfer kinetics originating from high tortuosity of Li^+/e^- transport pathways in the thick electrode (> 70μm). Over the past few years, relentless efforts have been devoted to improving solid-solid contact at the electrode-electrolyte interface,[36] preventing interfacial side reactions [9, 18, 64] and designing thick solid-state electrodes with fast electrochemical reaction kinetics.[65] Many review papers have discussed interface challenges in ASSBs.[20, 66] Here, we focus on promising manufacturing

11

processes for thick solid-state electrodes (**Figure 3**), including tape casting,[67] soluble/melt SSE infiltration, [31, 68] and dry electrode technology.[24, 28, 69]
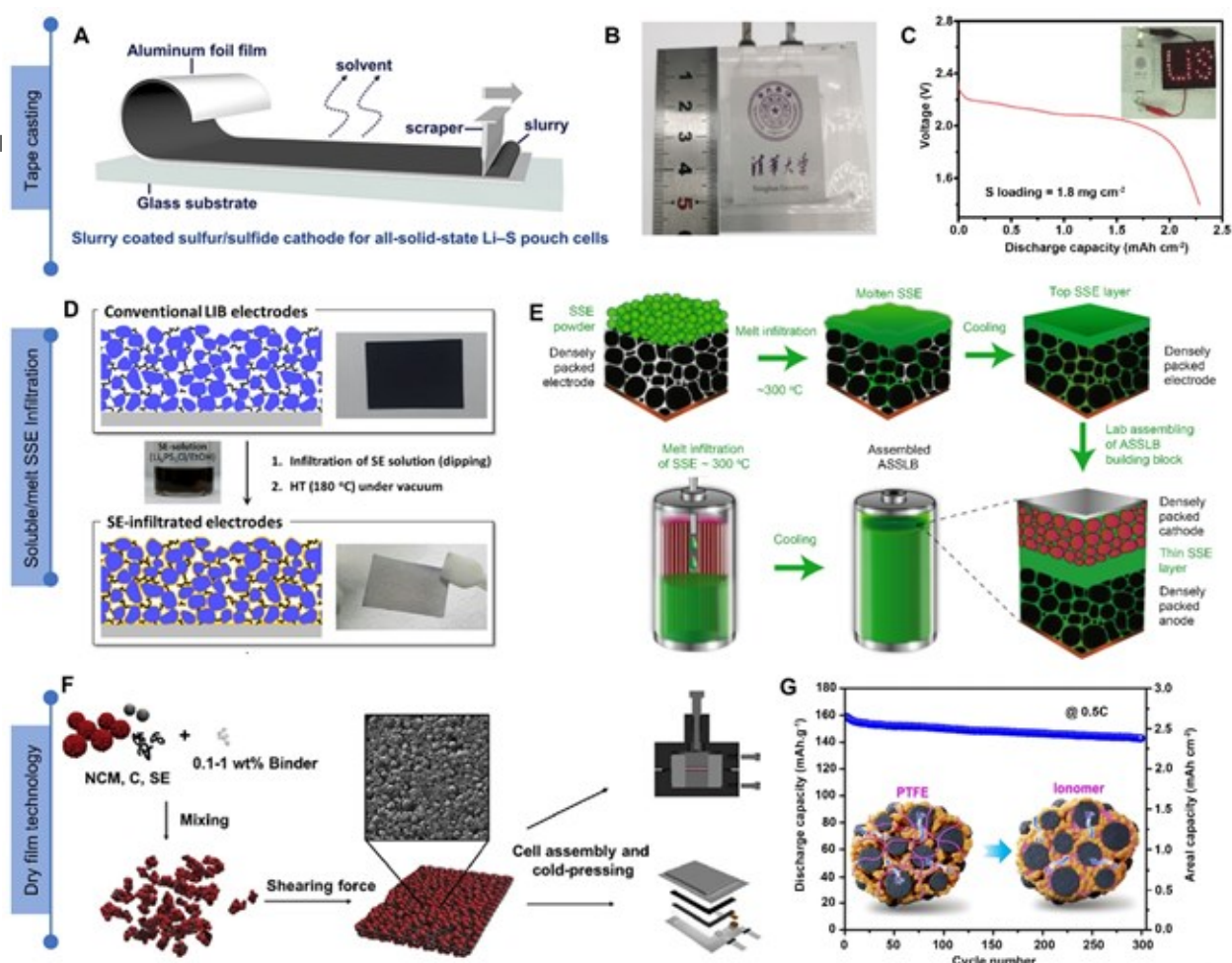
Figure 3. Advanced technologies for fabricating sheet-type cathodes for all-solid-state pouch cells. (**A**) Schematic for preparation of solid sulfur electrode film by the slurry coating process. (**B**) A photo of all-solid-state Li-S pouch cells. (**C**) A discharge curve of all-solid-state Li-S pouch cells with a sulfur loading of 1.8 mg.cm^{-2}. Adapted with permission from ref.[67] Copyright©2020, Wiley. (**D**) Schematics of infiltrating soluble SSEs into traditional electrodes. Adapted with permission from ref.[31]. (**E**) Schematic illustration of melt infiltration strategy. Adapted with permission from ref.[68] (**F**) Schematic diagram of a dry-film process to fabricate sheet-type cathode electrodes. Adapted with permission from ref.[24] (**G**) Cycling stability of $LiNi_{0.7}Co_{0.1}Mn_{0.2}O_2$ cathode composites fabricated by a Li^+-conducting ionomer binder. Adapted with permission from ref. [62] Copyright©2022, ACS.

Establishing a scalable manufacturing scheme for thick solid-state electrodes is challenging because of the chemical sensitivity of SSEs, especially solvent-sensitive sulfides

and halides.[10, 70] Tremendous efforts have been made to screen solvents and binders that are compatible with inorganic SSEs. For example, Q. Zhang et al. successfully fabricated a sheet-type solid-state sulfur electrode for all-solid-state Li-S pouch cells (**Fig. 3A** and **3B**) by the screening of various solvents and appropriate binder contents,[67] delivering a discharge capacity of 2.3 mAh.cm^{-2} (**Fig. 3C**). Y-S Jung and co-workers fabricated an 8×6 cm^2 all-solid-state pouch cell using a sulfide SSE via the tape-casting process. Apart from the typical tape-casting process, Y-S Jung et al. developed a series of soluble sulfide SSEs, which can be infiltrated into conventional sheet-type electrodes via a dip-coating process. Followed by isostatic pressing, all-solid-state batteries can be realized (**Fig. 3D**).[31] It should be highlighted that this soluble SSE dip coating process is compatible with existing LIB fabrication processes. Recently, G. Yushin et al. demonstrated a melt-infiltration strategy for scalable ASSB fabrication (**Fig. 3E**).[68] They utilized SSEs with low melting (~300 °C or below) points that can be infiltrated into electrodes at moderately elevated temperatures in a liquid state, which can solidify solid-state electrodes during cooling.[68]

With the potential to streamline production while addressing problems with the traditional slurry casting method, including solvent sensitivity and ion-transport blockage, dry electrode technology that can offer a "powder to film" path is gaining attention from both academia and industry.[58, 69] In addition, the wet-chemistry process faces a challenge in fabricating thick high-capacity electrodes. To realize thick electrodes, solvent-free dry electrode technology has been applied to fabricate thick solid-state electrodes for ASSB manufacturing.[58, 69] Recently, we engineered the first all-solid-state pouch cell prototype using a bilayer SSE (halide Li$_3$InCl$_6$+sulfide Li$_6$PS$_5$Cl), exhibiting excellent electrochemical performance and safety.[28] We also fabricated a quasi-solid-state pouch cell with a 20μm LLZTO membrane, demonstrating a high energy density of 280 Wh.kg^{-1} and a high capacity retention of 94.4% after 250 cycles.[28] F. Hippauf et al. utilized a dry film process to develop a 3×3 cm^2 all-solid-state pouch cell using a sulfide SSE (Li$_6$PS$_5$Cl),[24] which exhibited stable cycling over 100 cycles (**Fig. 3F**).[24] B. Ludwig and co-workers proposed a new dry powder painting process, which has better economic benefits and shows greater adhesion force with current collectors compared to the conventional slurry coating process.[71] Currently, dry electrode technology mainly relies on the fabrication of PTFE, a polymer that is reactive with Li metal.[50] Although some other binders, such as styrene‐butadiene rubber (SBR) and silicone rubber, have also been attempted for the dry-film process in 2003,[72] their viscosities are not as good as PTFE. Recently, a new chemical process was developed to improve the

binder property of styrene‐butadiene rubber (SBR) for the dry-film process.[73] Most polymer binders in the composite electrode are ionically insulative, which restricts the ion transport of thick electrodes. To resolve this issue, a Li^+-conducting ionomer binder poly(tetrafluoroethylene-co-perfluoro(3-oxa-4-pentenesulfonic acid)) lithium salt was designed for the solvent-free dry film process, demonstrating excellent Li+ transport and good interfacial contact in composite electrodes consisting of $LiNi_{0.7}Co_{0.1}Mn_{0.2}O_2$, conducting carbon, and Li_6PS_5Cl during cycling (**Fig. 3G**).[62] Also, the mechanical strength of sheet-type solid-state electrodes and SSE membranes manufactured by dry film technology should also be carefully investigated. Moreover, new facilities and compatibility with existing LIB production facilities should be developed and considered.

2.3.2 Innovative diffusion-dependent solid-state electrodes
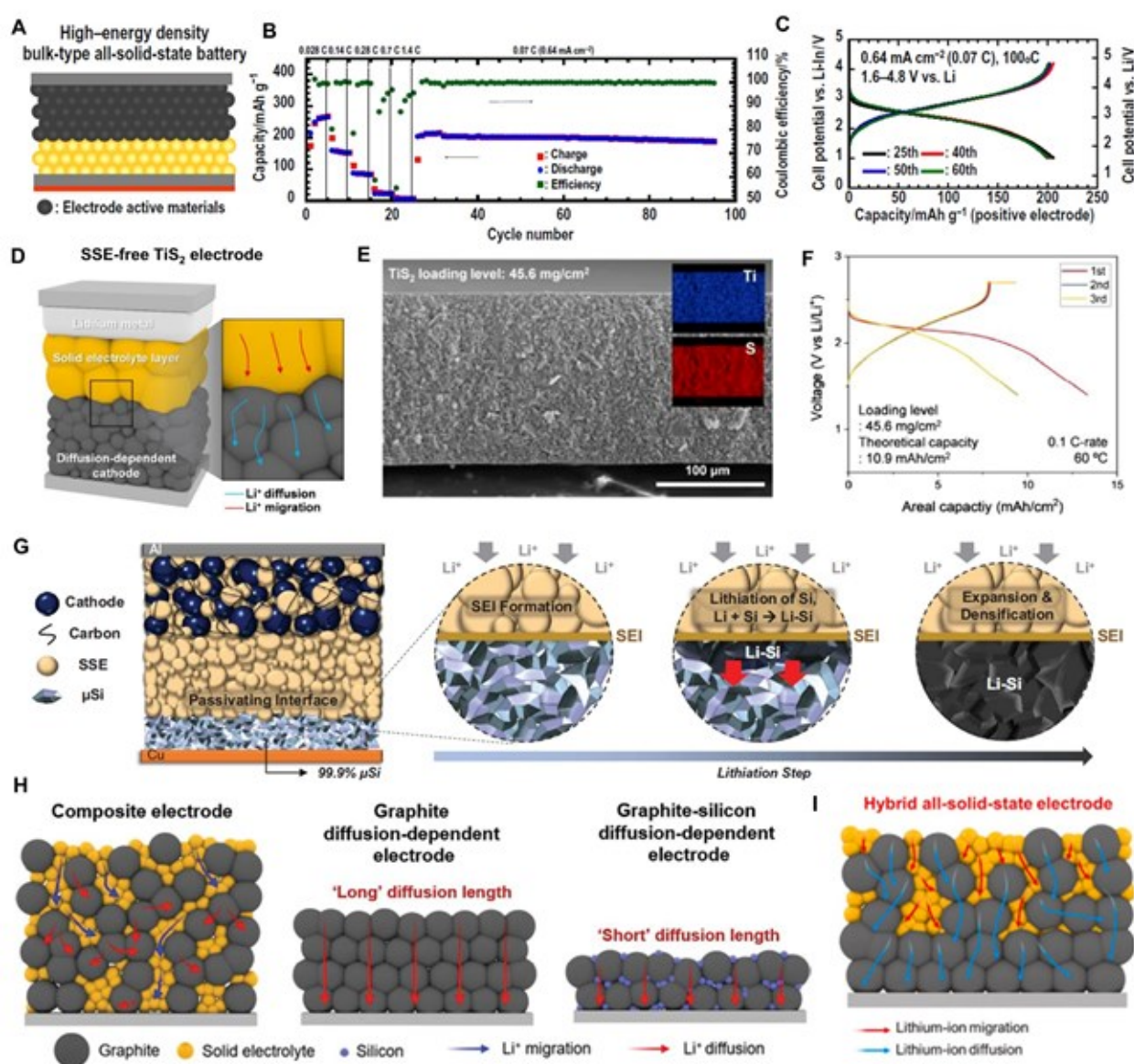
Figure 4. Diffusion-dependent solid-state electrode with high areal capacity. (**A**) Schematic for the high energy density of bulk-type all-solid-state batteries. The positive electrode layer is composed only of active material, which is the ideal battery configuration for high energy density. (**B**) Charge-discharge curves of the all-solid-state cell operated under the constant current density of 0.25 mA cm^{-2} (0.028 C rate) at 100°C. (**C**) Charge-discharge performance under the operation of various current densities. Adapted with permission from ref.[74] Copyright©2020, AAAS. (**D**) Schematic illustration of the all-solid-state lithium battery employing the TiS$_2$ diffusion-dependent cathode. (E) cross-sectional SEM image of the pelletized electrode of ball-milled TiS$_2$. (**F**) Charge-discharge voltage profiles of ball-milled TiS$_2$ diffusion-dependent electrode. Adapted with permission from ref.[75]. Copyright©2021**,** Elsevier. (**G**) Schematic of 99.9 wt % μSi electrode in an ASSB full cell. During lithiation, a passivating SEI is formed between the μSi and the SSE, followed by the lithiation of μSi particles near the interface. The highly reactive Li-Si then reacts with Si particles within its vicinity. The reaction propagates throughout the electrode, forming a densified Li-Si layer. Adapted with permission from ref.[76], Copyright©2021, AAAS. (**H**) Schematic illustration of the structure and lithium-ion transport of the composite electrode, the graphite diffusion-dependent electrode, and the graphite–silicon diffusion-dependent electrode. Adapted with permission from ref.[77], Copyright©2021, Wiley. (**I**) Schematic illustration of Li-ion transport mechanism in a composite-diffusion hybrid electrode. Adapted with permission from ref.[78], Copyright©2022. Elsevier.

In a typical thick composite electrode, SSEs and conductive agents are added to construct an ion and electron transport network. The active material content in the composite electrode is usually about 70%~85%, which limits the energy density of all-solid-state pouch cells. Recently, an innovative concept of diffusion-dependent solid-state electrodes has been reported in which no SSE is added to the electrode. This strategy maximizes energy density and simultaneously relieves the concerns about chemical reactivity between inorganic SSEs and solvents/binders that are indispensable for sheet-type electrode fabrication.[79] Furthermore, many challenges originating from the composite electrodes, such as interfacial side reactions between electrode materials and SSEs, SSE decomposition caused by carbon additives, and extra surface coating on active materials, are prevented. Consequently, diffusion-dependent solid-state electrodes have demonstrated higher areal capacity and better

cycling stability than classic composite electrodes, despite an elevated temperature (60~80°C) required to facilitate Li-ion diffusion in diffusion-dependent electrodes.[74-77]

Inspired by these advantages, tremendous efforts have been devoted to developing diffusion-dependent solid-state cathodes and anodes. For instance, A. Sakuda et al. designed an ion and electron mixed conductor as the cathode material ($Li_2Ru_{0.8}S_{0.2}O_{3.2}$) for ASSBs,[74] where the $Li_2Ru_{0.8}S_{0.2}O_{3.2}$ does not require any extra carbon additives or SSEs (**Fig. 4A**). The diffusion-dependent electrode exhibits satisfactory rate performance and a high reversible capacity of about 200 mAh.g^{-1} under a current density of 0.64 mA.cm^{-2} (**Fig. 4B**). This capacity exceeds the theoretical capacity of $Li_2Ru_{0.8}S_{0.2}O_{3.2}$ (141 mAh.g^{-1}), which is related to the anionic oxygen redox reaction in addition to the Ru^{5+}/Ru^{4+} redox reaction. The Coulombic efficiency reaches up to 99.8%, indicating the high reversibility of anionic oxygen redox reactions. The overlapping and negligible voltage decay of charge/discharge curves at different cycles also reveals the high reversibility of $Li_2Ru_{0.8}S_{0.2}O_{3.2}$ diffusion-dependent electrode in ASSBs (**Fig. 4C**). In another study, Y. Lee et al. designed a diffusion-dependent solid-state TiS_2 electrode (**Fig. 4D**), which delivers high areal and volumetric capacities of ~ 9.43 mAh.cm^{-2} and ~ 578 mAh.cm^{-3}, respectively, at a loading level of 45.6 mg.cm^{-2} (**Fig. 4E and 4F**). This excellent performance is attributed to the excellent mechanical ductility, high electronic conductivity, and stable Li-ion storage capability realized by the morphological change of TiS_2 from two-dimensional flakes to zero-dimensional nanograins.[75]

Along with the cathode, diffusion-dependent solid-state anodes have also been developed. For example, S. Meng's group reported a micro silicon diffusion-dependent electrode for ASSBs by virtue of high electronic conductivity (~3×10^{-5} S.cm^{-1}) of micro silicon and high Li-ion diffusivity of Li-Si (**Fig. 4G**). This micro silicon solid-state electrode exhibited a high reversible capacity of 2 mAh.cm^{-2} with a high capacity retention of 80% after 500 cycles.[76] However, high pressure is required, which needs to be reduced for commercialization. Y. Lee's group made great efforts in this direction. In 2020, his group first proposed a diffusion-dependent graphite electrode using a conventional slurry casting method. Utilizing Li-ion self-diffusion inside graphite electrodes, an areal capacity of 2~ 6 mAh.cm^{-2} can be obtained under an elevated temperature in a high-loading graphite electrode.[79] Following this work, they further presented a graphite-silicon diffusion-dependent electrode with a short effective diffusion length for ASSBs (**Fig. 4H**).[77] Recently, a hybrid solid-state electrode (composite electrode and diffusion electrode) strategy exhibited

high normalized capacities of 5.83 mA h cm^{-2} and 1300 mA h cm^{-3}, which are among the highest values reported to date for all-solid-state batteries.[78]

Diffusion-dependent solid-state electrodes provide a promising avenue for developing high-energy-density ASSBs. The key challenge is how to reduce the required pressure and operating temperature. We believe there are still many materials that can be designed and applied for diffusion-dependent electrodes. Currently, many studies report the electrochemical performance of diffusion-dependent electrodes at elevated temperatures (60°C~100°C) because of limited ion transport kinetics. Therefore, seeking and designing new electrode materials with high Li-ion diffusivity and excellent electronic conductivity so that ASSBs with diffusion-dependent electrodes can operate at room temperature or even low temperature is encouraged in the future.

2.4 Bipolar stacking of all-solid-state pouch cells
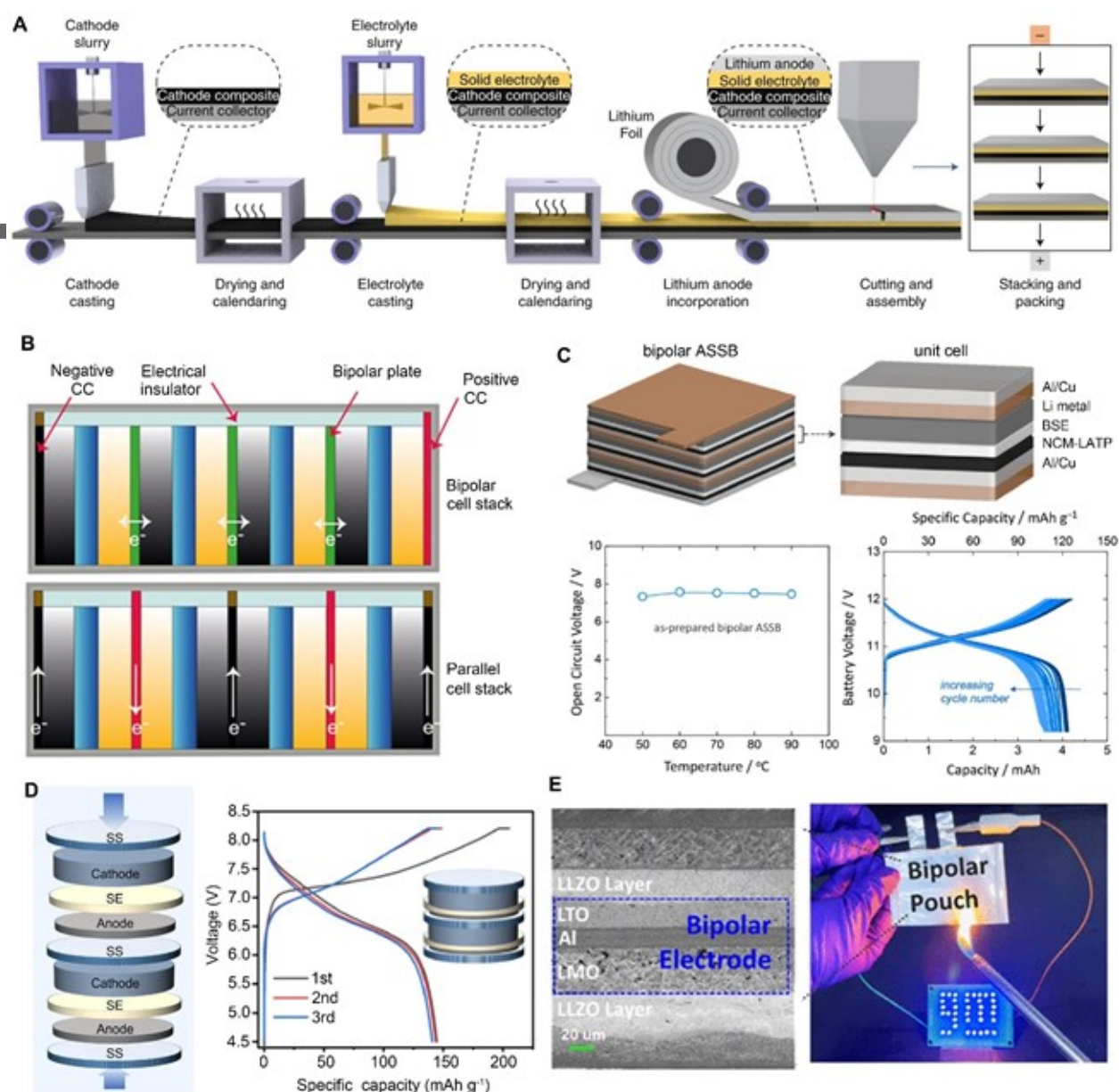
Figure 5. (A) Schematic of large-scale manufacturing of ASSBs. Adapted with permission from ref. Copyright © 2020, Nature.[80] **(B)** Schematic illustration of bipolar stacking compared to parallel stack. Adapted with permission from ref.[81]. Copyright©2021, ECS. (**C**) The open-circuit voltage (OCV) plot versus temperature for the three-cell bipolar ASSB with a biphasic SSE (LLTO+PEO) and its galvanostatic charge-discharge profiles. Adapted with permission from ref.[82] Copyright©2018, Wiley. (**D**) Charge/discharge curves of bipolar-stacked ASSB with sulfide SSE (Li$_6$PS$_5$Cl). Adapted with permission from ref.[83]. Copyright©2022. (**E**) Cross-sectional SEM image of the pouch-type LMO/LLZO−LTO bipolar solid-state battery wetted by the ionogel at the interface and powering a 5V blue LED. Adapted with permission from ref.[84] Copyright©2022, ACS.

With great success in thin SSE membranes and thick solid-state electrodes, all-solid-state pouch cells can be fabricated via a roll-to-roll process and assembled by bipolar stacking, as shown in **Fig. 5A**.[80] Unlike conventional LIBs that require each unit to be packed and then connected in series to form a module, all-solid-state batteries can use bipolar stacking to realize high voltage, thus providing provide significant benefits in terms of safety, thermal management, energy density, and cost.[81, 85, 86] Generally, there are two configurations of all-solid-state pouch cells (**Fig. 5B):** bipolar and parallel stacking. In bipolar stacking, each unit cell is connected in series through the bipolar plate (BP). Cathode materials are coated on one side of the plate, while anode materials are coated on the opposite side of the plate. The electron flows from one unit cell to the adjacent through the BP. In this case, the plate must be chemically and electrochemically stable with both cathode and anode materials. In a parallel stack, two electrodes with current collectors are separated by SSE membranes. Electrons flow in-plane along the current collector to the external tabs.[81] G. Offer et al. compared a bipolar and a parallel stack and found that Joule heating effects are negligible for bipolar stacks but are dominant for parallel stacks, which indicates that the bipolar stack is preferred for the simple thermal management system.[81]

Several review papers have summarized recent progress on bipolar stacking technologies.[81, 85, 86] Here, we show several examples of bipolar stacking with different SSEs. J-W Lee et al. demonstrated a proof-of-concept bipolar-stacked ASSB using a biphasic solid electrolyte membrane consisting of inorganic $Li_{0.29}La_{0.57}TiO_3$ and poly (ethylene oxide) and Al/Cu-cladded bipolar plates (**Fig. 5C**). With three cells connected in series, this bipolar-stacked ASSB exhibited a stable output voltage of 7.6V under different temperatures, indicating no short-circuiting and excellent thermal stability. Furthermore, this bipolar-stacked ASSB exhibited stable operation in a voltage range of 9.2V~12V at 60°C, delivering a specific capacity of 125 mAh.g^{-1} and a capacity retention of 83% over 50 cycles.[82] Based on sulfide SSE membranes, H. Zhu and her colleagues constructed bipolar stacked ASSBs, which deliver a high voltage of 8.2 V and cell-level energy density of 204 Wh kg^{-1}, much higher than that of a single cell (189 Wh kg^{-1}) (**Fig. 5D**).[83] With an in-situ formed non-flammable ion gel at the particle-to-particle interface, Z. Li et al. constructed a bipolar-stacked solid-state pouch cell with two cells connected in series, which exhibited superior power capability and functioned well at various temperatures (i.e., 0, −10, and −18 °C).[84] Recently, a 24V bipolar lithium metal pouch cell was demonstrated with an ultrathin solid polymer electrolyte (8 μm), which is fabricated by in-situ polymerization of carbonate ester

vinyl ethylene carbonate and poly(ethylene glycol) diacrylate on commercial porous polypropylene membrane.[87]

Though bipolar stacking technology can enable ASSBs with high energy density, good thermal stability, and high power density, bipolar stacking for all-solid-state pouch cells is still in its infancy because several technical challenges remain unresolved.[85] First, new (electro)chemically stable current collectors compatible with both cathode and anode materials should be developed, such as bi-layered bipolar plates and dual-metal cladded plates. Second, a proper thermal management system should be developed for bipolar stacked ASSBs. Third, an advanced stacking design with high precision should be developed to efficiently fabricate bipolar stacked all-solid-state pouch cells without internal circuit shorts.
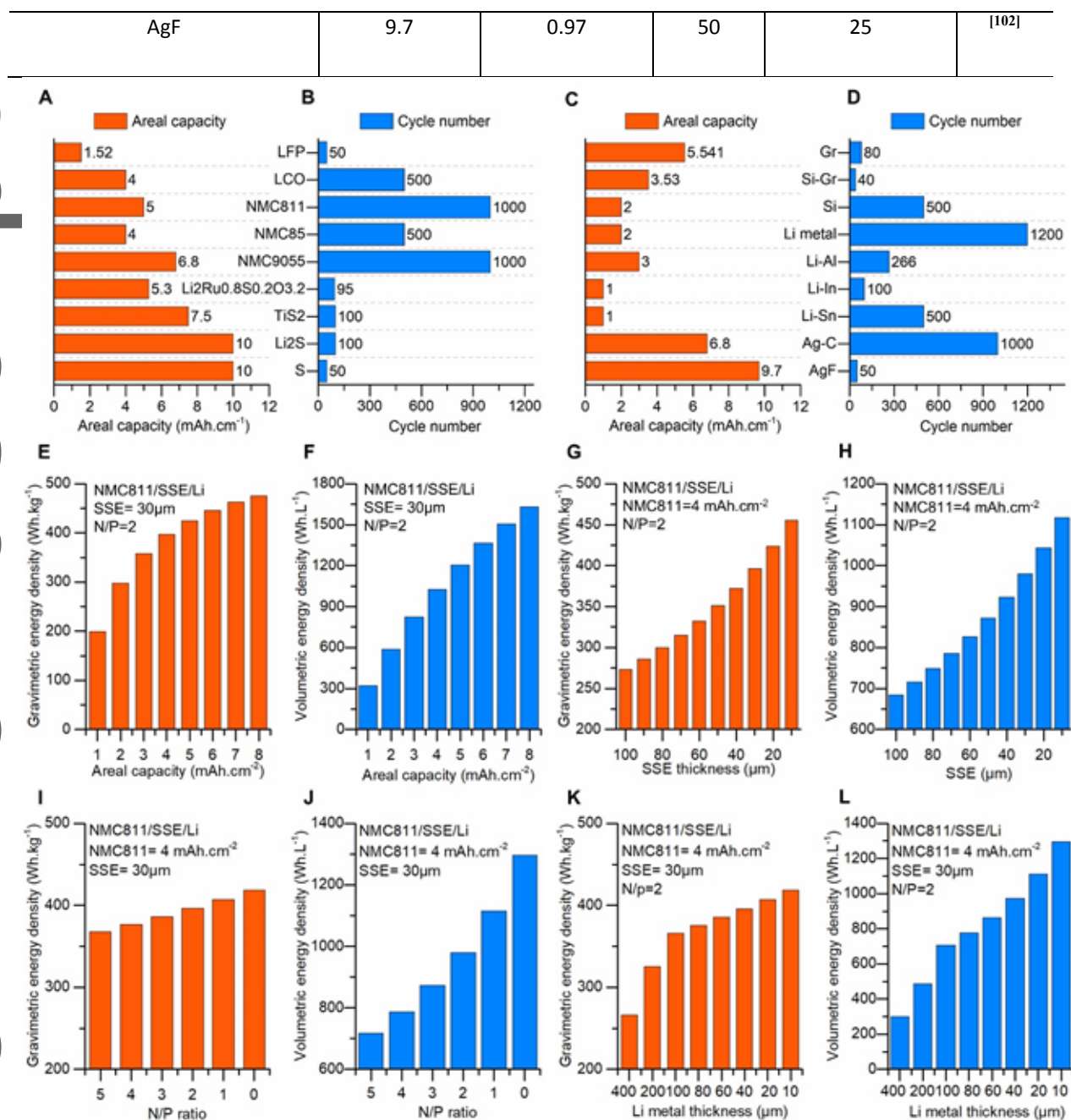
Other than bipolar stacking, other parameters, including manufacturing scalability,[88] process cost,[89] fabrication and testing pressure[90, 91] have also been investigated for ASSBs. Recent studies have shown fabrication pressure has a significant influence on material utilization because of its effect on the porosity of electrodes and SSEs.[90] In addition, increasing external testing pressure is usually beneficial for the long-term cycling stability of ASSBs, especially using large-volume-change electrode materials (e.g., silicon, sulfur, selenium).[76, 92] However, different materials have various mechanical properties, thus requiring skillful fabrication design for achieving intimate interfacial contact while preventing fabrication failures.[15] This would be more challenging when using ultrathin SSE membranes. Furthermore, pressure-effect on the electrochemical lithium deposition and stripping is expected to be studied in ASSBs.[93] Now it seems like both high fabrication pressure and high operation pressure is required for all-solid-state pouch cells. However, these high-pressure processes and inert fabrication environments undoubtedly increase the cost and low manufacturing efficiency.[89] Therefore, innovative strategies to reduce pressure and improve fabrication efficiency should be developed in the future.

Regarding temperature, more of the ASSBs reported in previous references were evaluated under room temperature or high temperature (60~100°C) with a low or moderate current density (0.1~1C) (**Table 2**). Comparatively, low-temperature and fast-charging ASSBs have not been fully developed, even though a few previous studies performed low-temperature or high-rate testing.[94] In addition, the testing protocol used for ASSBs is primarily constant current charging and discharging. The effect of the constant voltage process on ASSB's performance has not been studied yet. Therefore, more efforts are needed to establish standard testing protocols for all-solid-state pouch cells,

2.5 Energy density of all-solid-state pouch cells

Table 2. Summary on solid-state electrodes with high areal capacity.

Solid-state positive electrode					
Electrode material	**Areal capacity (mAh.cm^{-2})**	**Current density (mA.cm^{-2})**	**Cycle life**	**Testing temperature**	**Ref.**
$LiFePO_4$ (LFP)	1.52	0.15	50	80	[95]
$LiCoO_2$ (LCO)	4	1.2	500	25	[16]
$LiNi_{0.8}Co_{0.1}Mn_{0.1}O_2$ (NMC811)	5	3	1000	60	[96]
$LiNi_{0.85}Co_{0.1}Mn_{0.05}O_2$ (NMC85)	4	0.49	500	25	[16]
$LiNi_{0.9}Mn_{0.05}Co_{0.05}O_2$ (NMC9055)	6.8	6.8	1000	60	[25]
$Li_2Ru_{0.8}S_{0.2}O_{3.2}$	5.3	0.64	95	100	[74]
TiS_2	7.5	2.18	100	60	[75]
Li_2S	10	0.5	100	25	[97]
S	7.8	0.12	10	25	[98]
Solid-state negative electrode					
Graphite (Gr)	5.541	0.5	80	60	[79]
Graphite-Silicon (Gr-Si)	3.53	0.353	40	60	[77]
Silicon (Si)	2	5	500	25	[76]
Li metal	2	2	1200	25	[99]
Li-Al	3	10	266	25	[98]
Li-In	1	1	100	25	[100]
Li-Sn	1	1	500	25	[101]
Ag-C	6.8	6.8	1000	60	[25]

| | AgF | 9.7 | 0.97 | 50 | 25 | [102] |

Figure 6. Energy density analysis of all-solid-state lithium-ion pouch cells (NMC811/SSE/Li, SSE=Li₃InCl₆). (**A**) Promising solid-state positive electrodes with high areal capacity and corresponding cycling numbers (**B**). LiFeO₄ (LFP),[95] LiCoO₂ (LCO),[16] LiNi₀.₈Mn₀.₁Co₀.₁O₂ (NMC811),[96] LiNi₀.₈₅Mn₀.₁Co₀.₀₅O₂(NMC85),[16] LiNi₀.₉Mn₀.₀₅Co₀.₀₅O₂ (NMC9055),[25] Li₂Ru₀.₈S₀.₂O₃.₂,[74] TiS₂,[75] Li₂S,[97] S.[98] (**C**) Solid-state negative electrodes with high areal capacity and corresponding cycling numbers. Graphite(Gr),[79] Silicon-graphite (Si-Gr),[77] Silicon (Si),[76] Li metal,[99] Li-Al,[98] Li-In,[100] Li-Sn,[101] Li-Gr,[103] Siver-carbon (Ag-C),[25] and metal fluorides (AgF).[102] (**D**). The influence of different parameters on both gravimetric energy density and volumetric energy density: (**E, F**) The

areal capacity of solid-state NMC811 electrodes (NMC811=200 mAh.g^{-1}); **(G, H)** SSE thickness; (H, I) N/P ratio; **(K, L)** Li metal thickness.

2.5.1 Electrochemical performance of solid-state electrodes and all-solid-state pouch cells

Table 2 summarizes the current progress on the electrochemical performance of typical solid-state electrodes reported in previous references. **Fig. 6A** and **6B** highlight the areal capacity and cycle life of various cathode materials in a solid-state configuration. Intercalation-type cathodes such as $LiNi_{0.7}Co_{0.2}Mn_{0.1}O_2$ (4.46 mAh.cm^{-2}),[46] $LiNi_{0.8}Mn_{0.1}Co_{0.1}O_2$ (NMC811),[96] and $LiNi_{0.9}Mn_{0.05}Co_{0.05}O_2$ (NMC9055)[25] have already demonstrated high areal capacity (> 4 mAh.cm^{-2}) and excellent cycling stability (>1000 cycles). Not only intercalation-chemistry-based all-solid-state lithium-ion batteries but conversion-chemistry-based solid-state electrodes also demonstrated high areal capacities of 7~10 mAh.cm^{-2} with 100 cycles, such as TiS_2,[75] Li_2S,[97] and S.[104] On the anode side, typical commercially available anode materials have been attempted in solid-state electrodes and presented satisfactory results (**Fig. 6C** and **6D**). For example, Gr and Si-Gr composite solid-state electrodes showed 3~6 mAh.cm^{-2} with excellent cycling stability based on diffusion-dependent electrode structure.[77, 79] It should be mentioned that diffusion-dependent solid-state electrodes were evaluated under elevated temperatures (60~100 °C) because of sluggish Li-ion transport kinetics.[26, 74] More impressively, a carbon-free high-loading Si solid-state electrode with an areal capacity of 2 mAh.cm^{-2} can be stably cycled over 500 cycles with a capacity retention over 80%. Li metal anodes have also demonstrated great success in ASSBs. For example, Y. Zhong et al. demonstrated stable Li metal cycling under a large capacity of 2 mAh.cm^{-2} for 2400 hours using garnet SSEs.[99] F. Zhao et al. reported stable Li metal cycling with a high capacity of 5 mAh.cm^{-2} using fluorinated sulfide SSE.[105] Along with the success of pure metallic Li anodes, Li alloy anodes such as Li-Al,[106] Li-In,[100] and Li-Sn.[101] have recently shown great progress in ASSBs. Among them, Li-Al alloys demonstrated excellent cycling stability with Li_6PS_5Cl under a high capacity of 3 mAh.cm^{-2} at a high current density of 10 mA.cm^{-2}.[98] Remarkably, silver-carbon (Ag-C) composite anodes have realized a capacity of 6.8 mAh.cm^{-2} for 1000 cycles, as demonstrated by Samsung.[25] Recently, J. W. Chio et al. exploited the conversion reaction of AgF for anode-less ASSBs and realized a high areal capacity of 9.7 mAh.cm^{-2} for 50 cycles. It should be mentioned that silver is a costly metal, which may not be beneficial for realizing the cost-effectiveness of all-solid-state pouch cells. These encouraging lab-scale demonstrations

literally inspire a new wave of developing enthusiasm to commercialize game-changing ASSBs with intrinsic safety and overwhelming energy density.

2.5.2 Energy density of all-solid-state NMC811/Li pouch cells

Using commercial standards as a baseline, we performed numerical analysis to examine various solid-state electrode parameters (i.e., areal capacity, SSE thickness, N/P ratio, and Li metal thickness) and their influence on the energy density of all-solid-state pouch cells. The energy density calculation method is the same as our previous reports.[18, 107] (1) **Areal capacity**: Evidently, high areal capacity leads to high energy density (**Fig. 6E** and **6F**). An areal capacity of less than 1 mAh.cm^{-2} limits the energy density of all-solid-state pouch cells below 200 Wh.kg^{-1}, even when using ultrathin SSE membranes and Li metal foils. To obtain a competitive energy density (> 400 Wh.kg^{-1}), the areal capacity of solid-state electrodes should reach 4 mAh.cm^{-2}. At 4 mAh.cm^{-2}, the volumetric energy density can reach 980 Wh.L^{-1}. Considering current LIB's roll-to-roll fabrication technology, a solid-state electrode with an areal capacity of 4 mAh.cm^{-2} is practically achievable when using NMC811 and Li$_3$InCl$_6$ as the cathode and SSE, respectively, with a mass ratio of 85%:15%. When the tap density of the cathode composite is 3.4 g.cm$^{-3,}$ and the mass loading is 26 mg.cm^{-2}, the cathode thickness is 77μm, which is close to the current LIB's technology. (2) **SSE thickness**: Setting 4 mAh.cm^{-2} solid-state electrode as the target, we further evaluate the influence of SSE thickness on the energy density. Generally, energy density decreases as the SSE thickness increases (**Fig. 6G** and **6H**). A 30μm SSE is required to achieve an energy density of 400 Wh.kg^{-1}. (3) **N/P ratio**: The N/P ratio is the areal capacity ratio between the negative and positive electrodes. Here we also evaluate the effect of the N/P ratio on the energy density of all-solid-state pouch cells. It turns out that, due to the low density (0.534 g.cm^{-3}) of Li metal, the N/P ratio has less of an influence on the gravimetric energy density than it does on the volumetric energy density (**Fig. 6I** and **6J**). When the N/P ratio goes to zero, such as in anode-free configurations, the volumetric energy density can reach up to 1300 Wh.L^{-1}. However, anode-free all-solid-state pouch cells have a stringent requirement on the Coulombic efficiency of Li metals with current collectors.[108] (4) **Li metal thickness:** So far, most studies have been carried out based on thick Li metal (> 400 μm) anodes in a mold cell, which is far from practical engineering and dilutes the energy density. To secure 400 Wh.kg^{-1}, 40 μm Li metal foil should be integrated into pouch cells (**Fig. 6K**). The corresponding

volumetric energy density is 980 Wh.L^{-1} (**Fig. 6L**). However, thin Li metal normally suffer from short cycle life because of its low Coulombic efficiency and dendrite formation. Therefore, it is important to adopt advanced strategies, such as a fluorinated interphase and LiF-rich interface with high interface energy,[109] to realize high Coulombic efficiency (ideally,>99.98%) and suppress lithium dendrite formation. Therefore, future efforts should be devoted to developing 4 mAh.cm^{-2} solid-state electrodes with ultralong cycling stability, 30μm SSE membranes with high ionic conductivity and excellent mechanical strength, and 40μm Li metal foils with ultrahigh Coulombic efficiency (>99.98%). In addition, advanced strategies to enable all-solid-state pouch cell cycling at low pressure are desirable.
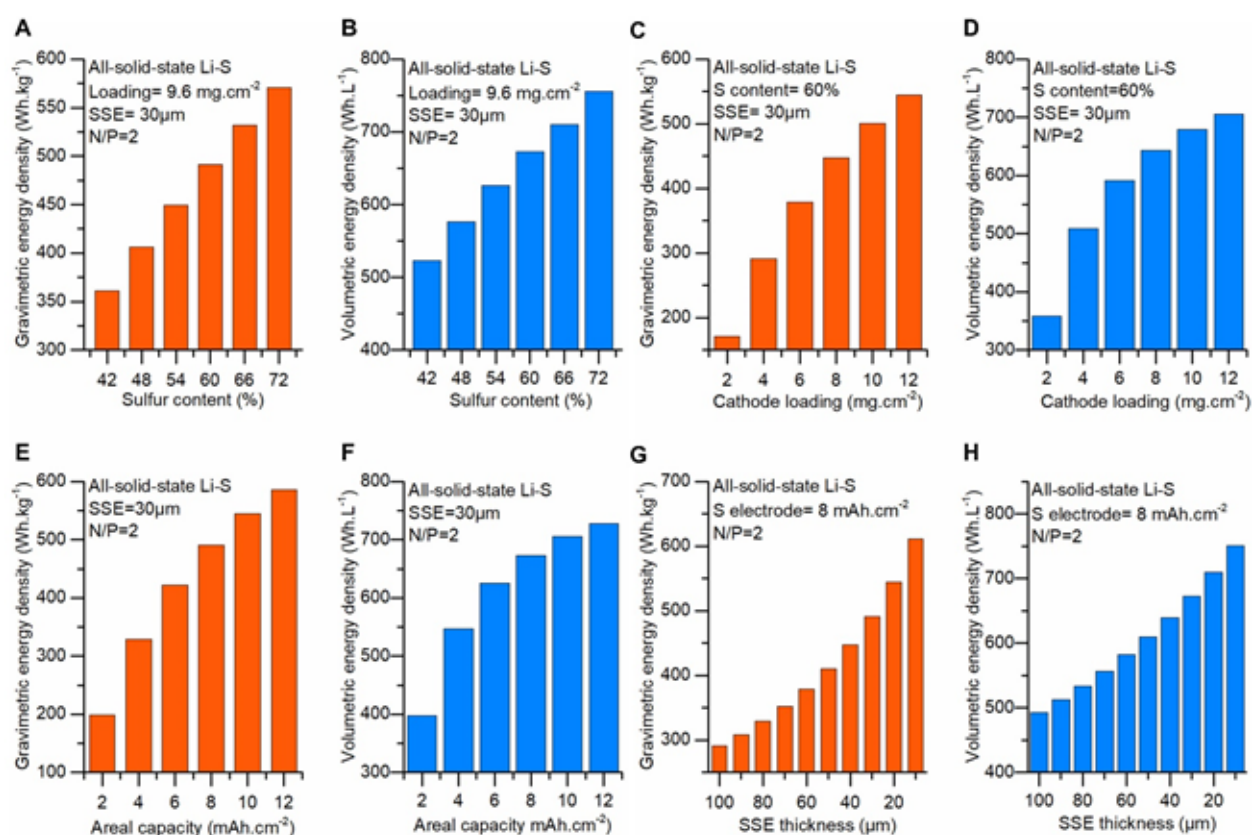
Figure 7. Energy density analysis of all-solid-state Li-S pouch cells (Sulfur + Carbon + SSE/SSE/Li, SSE=Li$_3$InCl$_6$). S=1400 mAh.g^{-1}.

### 2.5.3 Energy density of all-solid-state Li-S pouch cells

All-solid-state lithium-sulfur (Li-S) batteries based on conversion chemistry possess a high theoretical energy density (2600 Wh.kg^{-1}) and low cost because of cost-effective and earth-abundant sulfur resources, thus being regarded as a disruptive energy storage technology. However, several grand challenges hinder the development of all-solid-state Li-S

batteries, including (1) the ionically and electronically insulative nature of sulfur (5×10^{-30} S cm^{-1} at 25 °C), (2) significant volume change-induced physical contact loss at the interface, (3) interfacial reactions and SSE degradation, and (4) Li dendrite issue.[9, 110] Over the past years, several practical strategies have been proposed to tackle these challenges. For example, homogeneously mixing sulfur with a proper amount of SSEs and conductive carbon can improve its discharge capacity and reversibility (a.k.a. conversion efficiency).[111] In addition, the sufficient interfacial tri-phase area between SSE, carbon, and sulfur is crucial for high active material utilization in all-solid-state Li-S batteries. To secure long-term cycling stability, external pressure is usually required to suppress the volume change.[92] Moreover, using high-voltage stable SSEs is beneficial for avoiding interfacial reactions and SSE degradation.[112] With these tremendous successes, solid-state S electrodes have already demonstrated high areal capacities in the range of 7 to 10 mAh.cm^{-2}.[75, 97, 104] as highlighted in **Table 2**. Thus, it is worth evaluating the gravimetric and volumetric energy densities of all-solid-state Li-S pouch cells.

Here we utilize several parameters, such as sulfur content in cathode composites, the mass loading of cathode composites, the areal capacity of solid-state S electrodes, and SSE thickness to evaluate the energy density of all-solid-state Li-S pouch cells. (1) **Sulfur content and utilization**: As shown in **Fig. 7A**, an energy density over 500 Wh.kg^{-1} can only be achieved when the sulfur content in the cathode composite is at least 60%, and the cathode material loading is 9.6 mg.cm^{-2}. The specific sulfur capacity is 1400 mAh.g^{-1}, corresponding to a high sulfur utilization of over 83.6%. The corresponding volumetric energy density is 670 Wh.L^{-1} (**Fig. 7B**). The low ratio of the volumetric to the gravimetric energy density of solid-state Li-S pouch cells stems from the low tap density of the sulfur electrodes.[113] (2) **Sulfur loading**: Other than sulfur content, the mass loading of cathode composites also significantly influences the attainable energy density of all-solid-state Li-S pouch cells. 10 mg.cm^{-2} cathode composites (S content=60%) are required for realizing 500 Wh.kg^{-1} all-solid-state Li-S batteries (**Fig. 7C**). The corresponding volumetric energy is around 680 Wh.kg^{-1}(**Fig. 7D**). (3**) Areal capacity**: Furthermore, the solid-state sulfur electrodes with an areal capacity of 8 mAh.cm^{-2} should be guaranteed to obtain 500 Wh.kg^{-1} (**Fig. 7E**) and 680 Wh.L^{-1} (**Fig. 7F**). (4) **SSE thickness**: Similarly, 30 μm thin SSE should also be realized for all-solid-state Li-S pouch cells (**Fig. 7G** and **7H**). Based on this analysis, we set a research target (sulfur content $\geq$ 60%, specific capacity $\geq$ 1400 mAh.g^{-1}, sulfur utilization $\geq$ 83.6% loading $\geq$ 10 mg.cm^{-2}, areal capacity $\geq$ 8 mAh.cm^{-2}, and ultrathin SSE$\leq$30 μm) for future efforts in the field of all-solid-state Li-S batteries. Li metal is essential in all-solid-state Li-S

batteries using elemental sulfur as the cathode. Therefore, thin Li metal foil with a thickness of 40~80 μm is desirable for Li-S batteries. Similarly, high Coulombic efficiency (>99.98%) is also essential for the long-cycling stability of all-solid-state Li-S pouch cells.

3. Summary and Perspectives
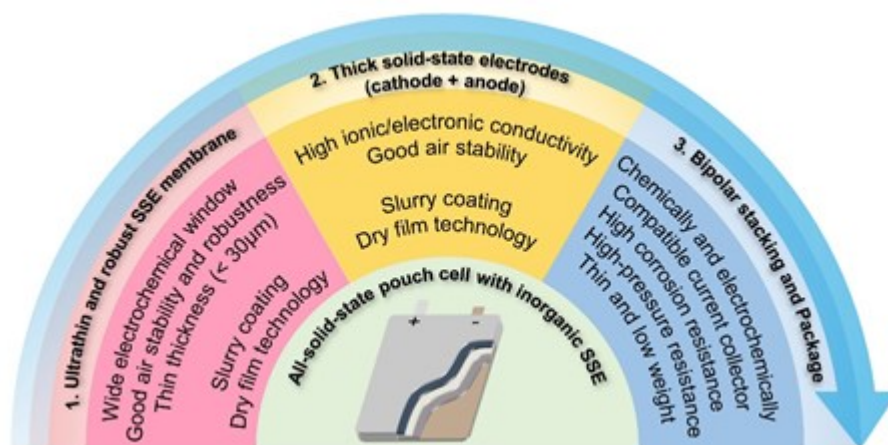
Figure 8. A summary of all-solid-state pouch cells

In summary, we provide a comprehensive overview of recent advancements in all-solid-state pouch cells, particularly with inorganic SSEs, covering thin and robust SSE membranes, thick solid-state electrodes with both composite electrode and innovative diffusion-dependent electrode microstructures, and bipolar stacking. In addition, critical engineering parameters (areal capacity, active material content and utilization, mass loading, SSE thickness, N/P ratio, and Li metal thickness) are thoroughly examined regarding their effect on the attainable energy density of all-solid-state pouch cells. Although substantial achievements have been made so far, there is still a long way to successfully realize industrial-able all-solid-state pouch cells with competitive energy density and inherent safety. Below are several promising directions to which future efforts should be devoted.

(1) Thin and robust SSE membranes

Developing thin and robust SSE membranes is crucial for attaining high energy density all-solid-state pouch cells. So far, most efforts have been devoted to decreasing the thickness of inorganic SSE membranes with decent ionic conductivity at room temperature. Other properties, such as low electronic conductivity, good electrochemical stability, and excellent mechanical flexibility, should not be ignored. A proper amount of polymeric binders seems necessary to obtain a thin, flexible, and robust SSE membrane, whether using a slurry coating

or a dry film process. As such, Li-ion conductive polymers that can be used as binders for SSE membrane fabrication are highly desired. Meanwhile, the SSE membrane's environmental stability (a.k.a, moisture stability) is crucial for industrial mass production. Therefore, developing air-stable SSEs membranes by directly synthesizing air-stable SSEs or designing a surface protection layer should be attempted.[114] Besides, exploring new (i.e., fluoride, mixed anions, and high entropy) anion framework-based superionic conductors with holistic properties exploiting is highly recommended.[115] Some fundamental questions, such as ion transport behavior across the inorganic and organic material interface are of great interest to investigate.[116]

(2) High-areal-capacity thick solid-state electrodes

Thick solid-state electrodes are a critical component in high-energy-density all-solid-state pouch cells.[65] Though several methods (i.e., tape casting, melt infiltration, and dry film technology) have been demonstrated to fabricate sheet-type thick solid-state electrodes, critical parameters that heavily influence the electrochemical performance of all-solid-sate pouch cells such as tape density, flexibility, porosity, and slurry viscosity are often overlooked. In addition, a standard protocol, including binders and solvents, should also be established in the future. As a guideline, thick solid-state electrodes with areal capacities ranging from 4 to 8 mAh.cm^{-2} and high utilization of active materials should be developed. Regarding diffusion-dependent solid-state electrodes, fast-charging electrode materials with high ion diffusivity at room temperature should be exploited. Besides, the influence of the volume change of active materials upon cycling on the electrochemical performance of ASSBs should be carefully examined, and proper strategies such as optimal external pressure should be defined.

(3) Bipolar stacking with bipolar plates

To achieve multi-layer all-solid-state pouch cells via bipolar stacking, bipolar plates should exhibit excellent (electro) chemical stability toward both the positive and negative electrodes. In this regard, metallic bipolar plates such as dual-metal cladded plates (not form alloys or compounds) and ultrathin Ti or stainless-steel plates are promising options. Furthermore, metallic bipolar plates should be corrosion-resistant to various SSEs, such as sulfides and halides. Finally, a suitable thermal management system should be developed to cater to bipolar-stacked ASSBs.

(4) Optimized pressure and wide temperature windows for ASSB operation.

Currently, many studies report ASSBs tested at room or high temperatures (25~100°C). However, the low-temperature performance of ASSBs should also be examined to resemble practical working conditions. In addition, the self-discharge behavior of all-solid-state pouch cells needs to be examined, particularly for their application in electric vehicles and grid-scale energy storage stations. ASSBs are often tested using high external pressure, which is often extremely challenging to reach for large-format all-solid-state pouch cells. Therefore, the optimized and viable pressure for the fabrication and operation of all-solid-state pouch cells should also be defined in the future.

Though the widespread adoption of all-solid-state pouch cells with high energy density, excellent safety, and good eco-efficiency remains far from fruition, we firmly believe that both the fundamental insights and practical perspectives discussed in this Review can help accelerate the commercial application of ASSBs.

References:

[1]   K. Liu, Y. Liu, D. Lin, A. Pei, Y. Cui, Sci. Adv. 2018, 4, eaas9820.

[2]   D. Chao, W. Zhou, F. Xie, C. Ye, H. Li, M. Jaroniec, S.-Z. Qiao, Sci. Adv. 2020, 6, eaba4098.

[3]   J. Wang, Y. Yamada, K. Sodeyama, E. Watanabe, K. Takada, Y. Tateyama, A. Yamada, Nat. Energy 2018, 3, 22.

[4]   M. Waqas, S. Ali, C. Feng, D. Chen, J. Han, W. He, Small 2019, 15, 1901689.

[5]   T. Famprikis, P. Canepa, J. A. Dawson, M. S. Islam, C. Masquelier, Nat. Mater. 2019; C. Wang, J. Liang, J. T. Kim, X. Sun, Sci. Adv. 2022, 8, eadc9516.

[6]   Y. Seino, T. Ota, K. Takada, A. Hayashi, M. Tatsumisago, Energy Environ. Sci. 2014, 7, 627.

[7]   M. Lei, S. Fan, Y. Yu, J. Hu, K. Chen, Y. Gu, C. Wu, Y. Zhang, C. Li, Energy Storage Mater. 2022, 47, 551.

[8]   Y. Kato, S. Hori, T. Saito, K. Suzuki, M. Hirayama, A. Mitsui, M. Yonemura, H. Iba, R. Kanno, Nat. Energy 2016, 1, 16030.

[9]   C. Wang, K. Adair, X. Sun, Acc. Mater. Res. 2022, 3, 21.

[10]   J. Lee, T. Lee, K. Char, K. J. Kim, J. W. Choi, Acc. Chem. Res. 2021, 54, 3390.

[11]   N. Boaretto, I. Garbayo, S. Valiyaveettil-SobhanRaj, A. Quintela, C. Li, M. Casas-Cabanas, F. Aguesse, J. Power Sources 2021, 502, 229919.

[12]   C. Singer, H.-C. Töpper, T. Kutsch, R. Schuster, R. Koerver, R. Daub, ACS Appl. Mater. Interfaces 2022, 14, 24245.

[13]   S. Lee, K.-s. Lee, S. Kim, K. Yoon, S. Han, M. H. Lee, Y. Ko, J. H. Noh, W. Kim, K. Kang, Sci. Adv. 2022, 8, eabq0153.

[14]   C. Wang, X. Li, Y. Zhao, M. N. Banis, J. Liang, X. Li, Y. Sun, K. R. Adair, Q. Sun, Y. Liu, F. Zhao, S. Deng, X. Lin, R. Li, Y. Hu, T.-K. Sham, H. Huang, L. Zhang, R. Yang, S. Lu, X. Sun, Small Methods 2019, 3, 1900261; Y. Zhang, J. Meng, K. Chen, H. Wu, J. Hu, C. Li, ACS Energy Lett. 2020, 5, 1167.

[15]   J. M. Doux, H. Nguyen, D. H. Tan, A. Banerjee, X. Wang, E. A. Wu, C. Jo, H. Yang, Y. S. Meng, Adv. Energy Mater. 2020, 10, 1903253.

[16]   L. Zhou, T.-T. Zuo, C. Y. Kwok, S. Y. Kim, A. Assoud, Q. Zhang, J. Janek, L. F. Nazar, Nat. Energy 2022, 7, 83.

[17]   M. J. Wang, E. Kazyak, N. P. Dasgupta, J. Sakamoto, Joule 2021, 5, 1371.

[18]   C. Wang, J. Liang, Y. Zhao, M. Zheng, X. Li, X. Sun, Energy Environ. Sci. 2021, 14, 2577.

[19]   J. Wu, L. Yuan, W. Zhang, Z. Li, X. Xie, Y. Huang, Energy Environ. Sci. 2021, 14, 12; X. Yang, K. R. Adair, X. Gao, X. Sun, Energy Environ. Sci. 2021, 14, 643.

[20]   L. Xu, S. Tang, Y. Cheng, K. Wang, J. Liang, C. Liu, Y.-C. Cao, F. Wei, L. Mai, Joule 2018.

[21]   T. Inada, T. Kobayashi, N. Sonoyama, A. Yamada, S. Kondo, M. Nagao, R. Kanno, J. Power Sources 2009, 194, 1085.

[22]   Y. J. Nam, S. J. Cho, D. Y. Oh, J. M. Lim, S. Y. Kim, J. H. Song, Y. G. Lee, S. Y. Lee, Y. S. Jung, Nano Lett. 2015, 15, 3317.

[23]   J. Schnell, T. Günther, T. Knoche, C. Vieider, L. Köhler, A. Just, M. Keller, S. Passerini, G. Reinhart, J. Power Sources 2018, 382, 160.

[24]   F. Hippauf, B. Schumm, S. Doerfler, H. Althues, S. Fujiki, T. Shiratsuchi, T. Tsujimura, Y. Aihara, S. Kaskel, Energy Storage Mater. 2019, 21, 390.

[25]   Y.-G. Lee, S. Fujiki, C. Jung, N. Suzuki, N. Yashiro, R. Omoda, D.-S. Ko, T. Shiratsuchi, T. Sugimoto, S. Ryu, J. H. Ku, T. Watanabe, Y. Park, Y. Aihara, D. Im, I. T. Han, Nat. Energy 2020, 5, 299.

[26]   Y. Lin, M. Wu, J. Sun, L. Zhang, Q. Jian, T. Zhao, Adv. Energy Mater. 2021, 11, 2101612.

[27]   S. Liu, L. Zhou, J. Han, K. Wen, S. Guan, C. Xue, Z. Zhang, B. Xu, Y. Lin, Y. Shen, L. Li, C.-W. Nan, Adv. Energy Mater. 2022, 12, 2200660.

[28]   C. Wang, R. Yu, H. Duan, Q. Lu, Q. Li, K. R. Adair, D. Bao, Y. Liu, R. Yang, J. Wang, S. Zhao, H. Huang, X. Sun, ACS Energy Lett. 2022, 7, 410.

[29]   A. Sakuda, K. Kuratani, M. Yamamoto, M. Takahashi, T. Takeuchi, H. Kobayashi, J. Electrochem. Soc. 2017, 164, A2474.

[30]   K. H. Park, D. Y. Oh, Y. E. Choi, Y. J. Nam, L. Han, J.-Y. Kim, H. Xin, F. Lin, S. M. Oh, Y. S. Jung, Adv. Mater. 2016, 28, 1874.

[31]   D. H. Kim, D. Y. Oh, K. H. Park, Y. E. Choi, Y. J. Nam, H. A. Lee, S.-M. Lee, Y. S. Jung, Nano Lett. 2017, 17, 3013.

[32]   D. H. Kim, H. A. Lee, Y. B. Song, J. W. Park, S.-M. Lee, Y. S. Jung, J. Power Sources 2019, 426, 143.

[33]   D. H. Kim, Y.-H. Lee, Y. B. Song, H. Kwak, S.-Y. Lee, Y. S. Jung, ACS Energy Lett. 2020, 5, 718.

[34]   Y. J. Nam, D. Y. Oh, S. H. Jung, Y. S. Jung, J. Power Sources 2018, 375, 93.

[35]   D. Y. Oh, D. H. Kim, S. H. Jung, J.-G. Han, N.-S. Choi, Y. S. Jung, J. Mater. Chem. A 2017, 5, 20771.

[36]   K. H. Park, Q. Bai, D. H. Kim, D. Y. Oh, Y. Zhu, Y. Mo, Y. S. Jung, Adv. Energy Mater. 2018, 8, 1800035.

[37]   D. Y. Oh, Y. J. Nam, K. H. Park, S. H. Jung, S.-J. Cho, Y. K. Kim, Y.-G. Lee, S.-Y. Lee, Y. S. Jung, Adv. Energy Mater. 2015, 5, 1500865; W. Cho, J. Park, K. Kim, J.-S. Yu, G. Jeong, Small 2019, 17, 1902138.

[38]   M. Balaish, J. C. Gonzalez-Rosillo, K. J. Kim, Y. Zhu, Z. D. Hood, J. L. M. Rupp, Nat. Energy 2021, 6, 227.

[39]   Z. Jiang, S. Wang, X. Chen, W. Yang, X. Yao, X. Hu, Q. Han, H. Wang, Adv. Mater. 2020, 32, 1906221.

[40]   B. Li, Q. Su, L. Yu, S. Dong, M. Zhang, S. Ding, G. Du, B. Xu, J. Membr. Sci 2021, 618, 118734.

[41]   T. Jiang, P. He, G. Wang, Y. Shen, C.-W. Nan, L.-Z. Fan, Adv. Energy Mater. 2020, 10, 1903376.

[42]   D. Cao, Q. Li, X. Sun, Y. Wang, X. Zhao, E. Cakmak, W. Liang, A. Anderson, S. Ozcan, H. Zhu, Adv. Mater. 2021, 33, 2105505.

[43]   G. Liu, J. Shi, M. Zhu, W. Weng, L. Shen, J. Yang, X. Yao, Energy Storage Mater. 2021, 38, 249.

[44]   J. M. Whiteley, P. Taynton, W. Zhang, S.-H. Lee, Adv. Mater. 2015, 27, 6922.

[45]   W. Ping, C. Wang, R. Wang, Q. Dong, Z. Lin, A. H. Brozena, J. Dai, J. Luo, L. Hu, Sci. Adv. 2020, 6, eabc8641.

[46]   S. Luo, Z. Wang, A. Fan, X. Liu, H. Wang, W. Ma, L. Zhu, X. Zhang, J. Power Sources 2021, 485, 229325.

[47]   H. Wang, Z. D. Hood, Y. Xia, C. Liang, J. Mater. Chem. A 2016, 4, 8091.

[48]   Z. D. Hood, H. Wang, A. S. Pandian, R. Peng, K. D. Gilroy, M. Chi, C. Liang, Y. Xia, Adv. Energy Mater. 2018, 8, 1800014.

[49]   D. H. S. Tan, A. Banerjee, Z. Deng, E. A. Wu, H. Nguyen, J.-M. Doux, X. Wang, J.-h. Cheng, S. P. Ong, Y. S. Meng, Z. Chen, ACS Appl. Energy Mater. 2019, 2, 6542.

[50]   Z. Zhang, L. Wu, D. Zhou, W. Weng, X. Yao, Nano Lett. 2021, 21, 5233.

[51]   J. Bian, H. Yuan, M. Li, S. Ling, B. Deng, W. Luo, X. Chen, L. Yin, S. Li, L. Kong, R. Zhao, H. Lin, W. Xia, Y. Zhao, Z. Lu, Front. Chem. 2021, 9.

[52]   G.-L. Zhu, C.-Z. Zhao, H.-J. Peng, H. Yuan, J.-K. Hu, H.-X. Nan, Y. Lu, X.-Y. Liu, J.-Q. Huang, C. He, J. Zhang, Q. Zhang, Adv. Funct. Mater. 2021, 31, 2101985.

[53]   X. Chen, W. He, L.-X. Ding, S. Wang, H. Wang, Energy Environ. Sci. 2019, 12, 938; R. Xu, J. Yue, S. Liu, J. Tu, F. Han, P. Liu, C. Wang, ACS Energy Lett. 2019, 4, 1073.

[54]   H. Shen, E. Yi, S. Heywood, D. Y. Parkinson, G. Chen, N. Tamura, S. Sofie, K. Chen, M. M. Doeff, ACS Appl. Mater. Interfaces 2020, 12, 3494.

[55]   R. Ye, N. Hamzelui, M. Ihrig, M. Finsterbusch, E. Figgemeier, ACS Sustain. Chem. Eng. 2022, 10, 7613.

[56]   C. Wang, J. Liang, J. Luo, J. Liu, X. Li, F. Zhao, R. Li, H. Huang, S. Zhao, L. Zhang, J. Wang, X. Sun, Sci. Adv. 2021, 7, eabh1896; X. Li, J. Liang, N. Chen, J. Luo, K. R. Adair, C. Wang, M. N. Banis, T. K. Sham, L. Zhang, S. Zhao, Angew. Chem. Int. Ed. 2019, 131, 16579; A. Miura, N. C. Rosero-Navarro, A. Sakuda, K. Tadanaga, N. H. H. Phuc, A. Matsuda, N. Machida, A. Hayashi, M. Tatsumisago, Nat. Rev. Chem. 2019, 3, 189.

[57]   B. Zhao, Y. Lu, B. Yuan, Z. Wang, X. Han, Mater. Lett. 2022, 310, 131463.

[58]   Y. Lu, C.-Z. Zhao, H. Yuan, J.-K. Hu, J.-Q. Huang, Q. Zhang, Matter 2022, 5, 876.

[59]   J.-K. Hu, H. Yuan, S.-J. Yang, Y. Lu, S. Sun, J. Liu, Y.-L. Liao, S. Li, C.-Z. Zhao, J.-Q. Huang, J. Energy Chem. 2022, 71, 612.

[60]   J. Xu, Y. Li, P. Lu, W. Yan, M. Yang, H. Li, L. Chen, F. Wu, Adv. Energy Mater. 2022, 12, 2102348.

[61]   X. Tian, B. Xin, Z. Lu, W. Gao, F. Zhang, RSC Adv. 2019, 9, 11220.

[62]   S.-B. Hong, Y.-J. Lee, U.-H. Kim, C. Bak, Y. M. Lee, W. Cho, H. J. Hah, Y.-K. Sun, D.-W. Kim, ACS Energy Lett. 2022, 7, 1092.

[63]   M. Yamamoto, Y. Terauchi, A. Sakuda, M. Takahashi, Sci. Rep. 2018, 8, 1212; A. Gogia, Y. Wang, A. K. Rai, R. Bhattacharya, G. Subramanyam, J. Kumar, ACS Omega 2021, 6, 4204.

[64]   R. Chen, Q. Li, X. Yu, L. Chen, H. Li, Chem. Rev. 2020, 120, 6820.

[65]   X. Yang, K. Doyle-Davis, X. Gao, X. Sun, eTransportation 2022, 11, 100152.

[66]   A. Banerjee, X. Wang, C. Fang, E. A. Wu, Y. S. Meng, Chem. Rev. 2020, 120, 6878.

[67]   H. Yuan, H.-X. Nan, C.-Z. Zhao, G.-L. Zhu, Y. Lu, X.-B. Cheng, Q.-B. Liu, C.-X. He, J.-Q. Huang, Q. Zhang, Batter. Supercaps. 2020, 3, 596.

[68]   Y. Xiao, K. Turcheniuk, A. Narla, A.-Y. Song, X. Ren, A. Magasinski, A. Jain, S. Huang, H. Lee, G. Yushin, Nat. Mater. 2021, 20, 984.

[69]   Y. Li, Y. Wu, Z. Wang, J. Xu, T. Ma, L. Chen, H. Li, F. Wu, Mater. Today 2022, 55, 92.

[70]   J. Lee, K. Lee, T. Lee, H. Kim, K. Kim, W. Cho, A. Coskun, K. Char, J. W. Choi, Adv. Mater. 2020, 32, 2001702.

[71]   B. Ludwig, Z. Zheng, W. Shou, Y. Wang, H. Pan, Sci. Rep. 2016, 6, 23150.

[72]   T. Inada, K. Takada, A. Kajiyama, M. Kouguchi, H. Sasaki, S. Kondo, M. Watanabe, M. Murayama, R. Kanno, Solid State Ion. 2003, 158, 275.

[73]   Y. Li, Y. Wu, T. Ma, Z. Wang, Q. Gao, J. Xu, L. Chen, H. Li, F. Wu, Adv. Energy Mater. 2022, 12, 2201732.

[74]   K. Nagao, Y. Nagata, A. Sakuda, A. Hayashi, M. Deguchi, C. Hotehama, H. Tsukasaki, S. Mori, Y. Orikasa, K. Yamamoto, Y. Uchimoto, M. Tatsumisago, Sci. Adv. 2020, 6, eaax7236.

[75]   J. Y. Kim, J. Park, S. H. Kang, S. Jung, D. O. Shin, M. J. Lee, J. Oh, K. M. Kim, J. Zausch, Y.-G. Lee, Y. M. Lee, Energy Storage Mater. 2021, 41, 289.

[76]   D. H. S. Tan, Y.-T. Chen, H. Yang, W. Bao, B. Sreenarayanan, J.-M. Doux, W. Li, B. Lu, S.-Y. Ham, B. Sayahpour, J. Scharf, E. A. Wu, G. Deysher, H. E. Han, H. J. Hah, H. Jeong, J. B. Lee, Z. Chen, Y. S. Meng, Science 2021, 373, 1494.

[77]   J. Y. Kim, S. Jung, S. H. Kang, J. Park, M. J. Lee, D. Jin, D. O. Shin, Y.-G. Lee, Y. M. Lee, Adv. Energy Mater. 2021, 12, 2103108.

[78]   J. Y. Kim, S. Jung, S. H. Kang, M. J. Lee, D. Jin, D. O. Shin, Y.-G. Lee, Y. M. Lee, J. Power Sources 2022, 518, 230736.

[79]   J. Y. Kim, J. Park, M. J. Lee, S. H. Kang, D. O. Shin, J. Oh, J. Kim, K. M. Kim, Y.-G. Lee, Y. M. Lee, ACS Energy Lett. 2020, 5, 2995.

[80]   D. H. S. Tan, A. Banerjee, Z. Chen, Y. S. Meng, Nat. Nanotech. 2020, 15, 170.

[81]   M.-C. Pang, Y. Wei, H. Wang, M. Marinescu, Y. Yan, G. J. Offer, J. Electrochem. Soc. 2020, 167, 160555.

[82]   H.-S. Shin, W.-G. Ryu, M.-S. Park, K.-N. Jung, H. Kim, J.-W. Lee, ChemSusChem 2018, 11, 3184.

[83]   D. Cao, X. Sun, Y. Wang, H. Zhu, Energy Storage Mater. 2022, 48, 458.

[84]   Z. Li, Y. Lu, Q. Su, M. Wu, X. Que, H. Liu, ACS Appl. Mater. Interfaces 2022, 14, 5402.

[85]   K.-N. Jung, H.-S. Shin, M.-S. Park, J.-W. Lee, ChemElectroChem 2019, 6, 3842.

[86]   M. Dixit, A. Parejiya, R. Essehli, N. Muralidharan, S. U. Haq, R. Amin, I. Belharouak, Cell Reports Physical Science 2022, 3, 100756.

[87]   X. Chen, C. Sun, K. Wang, W. Dong, J. Han, D. Ning, Y. Li, W. Wu, C. Yang, Z. Lu, J. Electrochem. Soc. 2022, 169, 090509.

[88]   K. J. Huang, G. Ceder, E. A. Olivetti, Joule 2021, 5, 564.

[89]   W. Zaman, K. B. Hatzell, Curr. Opin. Solid State Mater. Sci. 2022, 26, 101003.

[90]   J.-M. Doux, Y. Yang, D. H. S. Tan, H. Nguyen, E. A. Wu, X. Wang, A. Banerjee, Y. S. Meng, J. Mater. Chem. A 2020, 8, 5049.

[91]   H. Choi, M. Kim, H. Lee, S. Jung, Y.-G. Lee, Y. M. Lee, K. Y. Cho, Nano Energy 2022, 102, 107679.

[92]   X. Li, J. Liang, X. Li, C. Wang, J. Luo, R. Li, X. Sun, Energy Environ. Sci. 2018, 11, 2828.

[93]   C. Fang, B. Lu, G. Pawar, M. Zhang, D. Cheng, S. Chen, M. Ceja, J.-M. Doux, H. Musrock, M. Cai, B. Liaw, Y. S. Meng, Nat. Energy 2021, 6, 987.

[94]   L. Peng, C. Yu, Z. Zhang, H. Ren, J. Zhang, Z. He, M. Yu, L. Zhang, S. Cheng, J. Xie, Chem. Eng. J. 2022, 430, 132896; S. Deng, M. Jiang, N. Chen, W. Li, M. Zheng, W. Chen, R. Li, H. Huang, J. Wang, C. V. Singh, X. Sun, Adv. Funct. Mater. 2022, 32, 2205594; S. Deng, M. Jiang, A. Rao, X. Lin, K. Doyle-Davis, J. Liang, C. Yu, R. Li, S. Zhao, L. Zhang, H. Huang, J. Wang, C. V. Singh, X. Sun, Adv. Funct. Mater. 2022, 32, 2200767.

[95]   X. Yang, Q. Sun, C. Zhao, X. Gao, K. R. Adair, Y. Liu, J. Luo, X. Lin, J. Liang, H. Huang, L. Zhang, R. Yang, S. Lu, R. Li, X. Sun, Nano Energy 2019, 61, 567.

[96]   S. Kim, J.-S. Kim, L. Miara, Y. Wang, S.-K. Jung, S. Y. Park, Z. Song, H. Kim, M. Badding, J. Chang, V. Roev, G. Yoon, R. Kim, J.-H. Kim, K. Yoon, D. Im, K. Kang, Nat. Commun. 2022, 13, 1883.

[97]   T. Hakari, Y. Fujita, M. Deguchi, Y. Kawasaki, M. Otoyama, Y. Yoneda, A. Sakuda, M. Tatsumisago, A. Hayashi, Adv. Funct. Mater. 2022, 32, 2106174.

[98]   Y. Huang, B. Shao, F. Han, J. Mater. Chem. A 2022, 10, 12350.

[99]   Y. Zhong, Y. Xie, S. Hwang, Q. Wang, J. J. Cha, D. Su, H. Wang, Angew. Chem. Int. Ed. 2020, 59, 14003.

[100]   A. L. Santhosha, L. Medenbach, J. R. Buchheim, P. Adelhelm, Batter. Supercaps. 2019, 2, 524.

[101]   C. Hänsel, B. Singh, D. Kiwic, P. Canepa, D. Kundu, Chem. Mater. 2021, 33, 6029.

[102]   J. Lee, S. H. Choi, G. Im, K.-J. Lee, T. Lee, J. Oh, N. Lee, H. Kim, Y. Kim, S. Lee, J. W. Choi, Adv. Mater. 2022, 34, 2203580.

[103]   L. Ye, X. Li, Nature 2021, 593, 218.

[104]   S. Xu, C. Y. Kwok, L. Zhou, Z. Zhang, I. Kochetkov, L. F. Nazar, Adv. Funct. Mater. 2021, 31, 2004239.

[105]   F. Zhao, Q. Sun, C. Yu, S. Zhang, K. Adair, S. Wang, Y. Liu, Y. Zhao, J. Liang, C. Wang, X. Li, X. Li, W. Xia, R. Li, H. Huang, L. Zhang, S. Zhao, S. Lu, X. Sun, ACS Energy Lett. 2020, 5, 1035.

[106]   H. Pan, M. Zhang, Z. Cheng, H. Jiang, J. Yang, P. Wang, P. He, H. Zhou, Sci. Adv. 2022, 8, eabn4372.

[107]   L. Liu, J. Xu, S. Wang, F. Wu, H. Li, L. Chen, eTransportation 2019, 1, 100010.

[108]   J. Xiao, Q. Li, Y. Bi, M. Cai, B. Dunn, T. Glossmann, J. Liu, T. Osaka, R. Sugiura, B. Wu, J. Yang, J.-G. Zhang, M. S. Whittingham, Nat. Energy 2020, 5, 561.

[109]   X. Fan, X. Ji, F. Han, J. Yue, J. Chen, L. Chen, T. Deng, J. Jiang, C. Wang, Sci. Adv. 2018, 4, 9245; X. Ji, S. Hou, P. Wang, X. He, N. Piao, J. Chen, X. Fan, C. Wang, Adv. Mater. 2020, 32, 2002741.

[110]   S. Ohno, W. G. Zeier, Acc. Mater. Res. 2021, 2, 869.

[111]   S. Ohno, R. Koerver, G. Dewald, C. Rosenbach, P. Titscher, D. Steckermeier, A. Kwade, J. Janek, W. G. Zeier, Chem. Mater. 2019, 31, 2930.

[112]   X. Li, J. Liang, J. T. Kim, J. Fu, H. Duan, N. Chen, R. Li, S. Zhao, J. Wang, H. Huang, X. Sun, Adv. Mater. 2022, 34, 2200856; X. Shi, Z. Zeng, M. Sun, B. Huang, H. Zhang, W. Luo, Y. Huang, Y. Du, C. Yan, Nano Lett. 2021, 21, 9325.

[113]   G. Zhou, H. Chen, Y. Cui, Nat. Energy 2022, 7, 312; W. Xue, L. Miao, L. Qie, C. Wang, S. Li, J. Wang, J. Li, Curr. Opin. Electrochem. 2017, 6, 92; Y.-T. Liu, S. Liu, G.-R. Li, X.-P. Gao, Adv. Mater. 2021, 33, 2003955.

[114]   P. Lu, D. Wu, L. Chen, H. Li, F. Wu, Electrochem. Energy Rev. 2022, 5, 3.

[115]   J. Hu, Z. Yao, K. Chen, C. Li, Energy Storage Mater. 2020, 28, 37; J. Lin, G. Cherkashinin, M. Schäfer, G. Melinte, S. Indris, A. Kondrakov, J. Janek, T. Brezesinski, F. Strauss, ACS Materials Lett. 2022, 4, 2187.

[116] M. R. Busche, T. Drossel, T. Leichtweiss, D. A. Weber, M. Falk, M. Schneider, M. L. Reich, H. Sommer, P. Adelhelm, J. Janek, Nat. Chem. 2016, 8, 426.

Dr. Changhong Wang is now a Banting Postdoctoral Fellow at the University of Maryland at College Park and a Visiting Researcher at Western University. He received his MS degree in Material Engineering from the University of Science and Technology of China in 2014 and his PhD degree in Mechanical and Material Engineering from the University of Western Ontario in 2020. His current research interests include all-solid-state batteries, solid electrolytes, lithium-sulfur batteries, solid-state pouch cells, and memristors.

Jung Tae (Justin) Kim is currently a graduate student in Prof. Xueliang Sun's research group at the University of Western Ontario, Canada. Justin received his BSc from the University of British Columbia in 2021. Currently, his research interests revolve around solid-state lithium-sulfur batteries.

Author Manuscript

Prof. Chunsheng Wang is Robert Franklin and Frances Riggs Wright Distinguished Chair Professor in the Department of Chemical & Biomolecular Engineering at UMD and a co-founder and UMD Director of the Centre for Research in Extreme Batteries (CREB), a joint battery research center between UMD and US Army Research Lab. His work has been cited more than 54000 times, with an H-index of 120. He has been recognized as a highly cited researcher by Clarivate since 2018. He was selected as the winner of the 2021 Battery Division Research Award by the Electrochemical Society.

Prof. Xueliang Sun is a Canada Research Chair in Development of Nanomaterials for Clean Energy, Fellow of the Royal Society of Canada and Canadian Academy of Engineering,, and Full Professor at the University of Western Ontario, Canada. Dr. Sun received his PhD in materials chemistry in 1999 from the University of Manchester, UK. He followed up by working as a postdoctoral fellow at the University of British Columbia, Canada and as a Research Associate at L′ Institut National de la Recherche Scientifique (INRS), Canada. His research interests focus on advanced materials for electrochemical energy storage and conversion.

Progress and Prospects of Inorganic Solid-State Electrolyte-Based All-Solid-State Pouch Cells

Changhong Wang[1,2], Jung Tae Kim[1], Chunsheng Wang[2,*], Xueliang Sun[1,*]

1. Department of Mechanical and Materials Engineering, University of Western Ontario, 1151 Richmond St., London, Ontario, N6A 3K7, Canada

2. Department of Chemical and Biomolecular Engineering, University of Maryland, College Park, MD 20740, USA

*Corresponding author: cswang@umd.edu; xsun9@uwo.ca

A short summary:

Research on all-solid-state batteries (ASSBs) is currently transitioning from lab-scale fundamental study to industry-scale application research. This review timely summarizes the current progress on inorganic solid-state electrolyte (SSE)-based all-solid-state pouch cells, analyzes their technical challenges, and outlines future research targets for realizing high-energy-density all-solid-state Li-ion and Li-S batteries.